Preprints.org

Concept Paper

Not peer-reviewed version

AI-Assisted Mathematical Results and Their Engineering Translation: An Evidence-Graded Review with Illustrative Electrical Engineering Numerical Studies

Mehdi Zeinali *

Posted Date: 23 November 2026

Keywords: artificial intelligence; mathematical discovery; theorem proving; Berger power inequality; Crouzeix–Palencia theorem; numerical radius; Ando LMI; p-cycle protection; MIMO detection; global inverse conditions; reproducible simulation

Preprints.org is a free multidisciplinary platform providing preprint service that is dedicated to making early versions of research outputs permanently available and citable. Preprints posted at Preprints.org appear in Web of Science, Crossref, Google Scholar, Scilit, Europe PMC, OpenAlex.

Copyright: This open access article is published under a Creative Commons CC BY 4.0 license, which permit the free download, distribution, and reuse, provided that the author and preprint are cited in any reuse.

Preprints.org | NOT PEER-REVIEWED | Posted: 23 November 2026 https://doi.org/10.20944/preprints202611.2339.v1

Disclaimer/Publisher's Note: The statements, opinions, and data contained in all publications are solely those of the individual author(s) and contributor(s) and not of MDPI and/or the editor(s). MDPI and/or the editor(s) disclaim responsibility for any injury to people or property resulting from any ideas, methods, instructions, or products referred to in the content.

Concept Paper

AI-Assisted Mathematical Results and Their Engineering Translation: An Evidence-Graded Review with Illustrative Electrical Engineering Numerical Studies

Mehdi Zeinali

School of Engineering, University of Hull, Hull HU6 7RX, United Kingdom; m.zeinali@hull.ac.uk

Abstract

This evidence-graded narrative review examines 51 AI-assisted mathematical findings, representing 49 distinct target families, including published theorems, formal proof artefacts, counterexamples, bounds, constructions and unverified announcements. Mathematical result type, evidence level and engineering relevance are classified separately; recent preprints are distinguished from established results. Four electrical engineering pathways are investigated: numerical-radius and matrix-polynomial certificates for inverter control, preconfigured protection cycles for resilient communications, complexity-aware finite-constellation MIMO detection, and measurement-projection design for nonlinear digital twins. Classical matrix-power bounds are attributed to Berger's inequality. For a two-state surrogate, Ando semidefinite synthesis is compared with spectral-norm and common-metric Lyapunov synthesis under a shared gain budget; direct spectral-norm minimisation gives the smallest observed amplification. The Crouzeix–Palencia polynomial certificate outperforms stronger classical baselines in only 3 of 300 two-dimensional and 2 of 100 four- and six-dimensional tests. Synthetic 2-by-2 16-QAM detection is evaluated on 10,000 channel frames per SNR with uncertainty intervals. A battery-inspired three-channel sensor model uses an a priori probabilistic noise envelope and a full-rank negative control. Six-state LCL and feeder-restoration studies provide exploratory checks. The findings identify both opportunities and limitations for translating AI-assisted mathematics into electrical engineering through established theory and reproducible numerical studies, without claiming new universal control theorems or physical validation.

Keywords: artificial intelligence; mathematical discovery; theorem proving; Berger power inequality; Crouzeix–Palencia theorem; numerical radius; Ando LMI; p-cycle protection; MIMO detection; global inverse conditions; reproducible simulation

1. Introduction: The Next Stage After AI Mathematics

1.1. Research Motivation

Mathematics supplies the guarantees that make engineering calculations reliable: stability of feedback systems, convergence of optimisation algorithms, minimum decoding distance, graph connectivity, identifiability of dynamical models, and upper limits on computational burden. Proofs of longstanding conjectures often require extensive specialist reasoning. AI tools now offer complementary capabilities for lemma search, symbolic exploration, proof formalisation, and computational verification. For example, the AI-driven formal-proof-search study by Tsoukalas *et al.* reports nine resolved statements from a set of 353 open Erdős problems and 44 proved conjectures from 492 On-Line Encyclopedia of Integer Sequences candidates [1]. Those counts concern the *particular tested collections*, not a world-wide total. Mathematical program search produced new cap-set constructions [2]; proof-guided research assisted in the 2026 sharp Crouzeix theorem claim [3,4], while the unconditionally published 2017 Crouzeix–Palencia theorem already provides a rigorous fallback constant for

© 2026 by the author(s). Distributed under a Creative Commons CC BY license.

Preprints.org | NOT PEER-REVIEWED | Posted: 23 November 2026 https://doi.org/10.20944/preprints202611.2339.v1

engineering design [5]; and independent mathematical expositions describe the AI-generated cycle double cover proof claim [6,7].

The engineering question is different: *what operation becomes newly possible, safer, easier to certify, cheaper or faster because the theorem is now available?* A hard theorem can be useful even if it provides a negative result. For example, a hardness proof limits universally guaranteed nearest-lattice-point approximations and prevents inappropriate claims of polynomial-time optimal MIMO decoding; a counterexample to a global-inverse conjecture warns against substituting local Jacobian rank for unique sensor inversion. For pure matrix powers the classical Berger inequality already supplies a factor-two bound; the genuinely more general Crouzeix framework concerns arbitrary analytic functions of matrices [5,8]. Both routes can motivate useful engineering research if novelty and limitations are stated precisely.

1.2. Scope and Contributions

This study addresses four connected questions. *What mathematical task was actually open? How did AI contribute to the reported solution or advance? What engineering domains could use the mathematical concept? What new electrical-engineering formulation can be implemented and tested?* The contributions are: (i) an evidence-graded audit of 51 findings and 49 named target families; (ii) explicit separation of classical theorems from reported 2026 results; (iii) four proposed, testable engineering translations without novelty claims for existing textbook results; (iv) reproducible numerical pilots and counterexamples; and (v) an engineering research priority matrix. The manuscript is a critical survey plus proposed methodology, not a claim that the proposed control, grid, radio, or sensing systems have already been experimentally validated.

1.3. Why "AI Solved" Needs Definition

Attribution should not overclaim either autonomy or novelty. AI can formulate candidate lemmas, search formal proof states, generate code, verify a finite certificate, rediscover an existing proof, or provide the key idea in a human-written paper. Those are materially different contributions. For instance, a *Lean-checked theorem* means the checked formal statement follows from the formal premises admitted into the proof environment; it does not independently establish that the authors transcribed the original historical question correctly or that every assumption matches the intended generality. Conversely, a rigorous, human-checked conventional proof can establish correctness without being Lean-checked. An improved exponent, an extra Hadamard matrix, or a lower-dimension counterexample is a genuine mathematical advance but does not mean that the broad underlying conjecture was solved.

2. Review Protocol, Taxonomy, and Evidence Limitations

2.1. Collection, Verification and Reproducibility Protocol

This is a *curated narrative review*, not a PRISMA-style systematic review. The review began with a predefined catalogue of 51 findings. The editorial audit checked source identifiers attached to those entries, targeted original journal and arXiv papers, the Erdős problems registry and formal-conjecture statements, independent mathematical expositions, and engineering baseline literature. Queries were of the forms "[named conjecture] proof", "[author] arXiv [identifier]", "[result] independent verification", "numerical radius Berger Ando LMI", and "optical p-cycle protection". The screening cutoff was 14 November 2026. Inclusion required a specific public claim, cited proof or reproducible construction; unsupported predictions were excluded. The bibliography and source audit list source identifiers; a public URL alone never upgrades a claim to independent verification. The numerical reference scripts were executed and their outputs checked against the stated formulas. Source identification does not constitute personal verification of every cited proof. This is a targeted audit of 51 included entries, not an exhaustive search. No external specialist refereeing or Lean proof build was performed in this study. The source access and status caveats are recorded in the supplementary audit and in Appendix C.

© 2026 by the author(s). Distributed under a Creative Commons CC BY license.

Preprints.org | NOT PEER-REVIEWED | Posted: 23 November 2026 https://doi.org/10.20944/preprints202611.2339.v1

2.2. Result Type, Evidence Level and Engineering-Link Taxonomy

Result type denotes **P** (proof or disproof of a stated claim by a theoretical argument), **X** (counterexample), **B** (improved bound or asymptotic rate), or **K** (explicit construction or computational record). A qualification of scope is recorded in the case notes and is not itself proof acceptance. **Evidence grade** denotes **E1** (a peer-reviewed publication *or* independent detailed written verification, distinguished in the case notes), **E2** (a public formal-proof artefact or exact certificate with a documented successful, version-specific build or exact check corroborated beyond a release announcement), and **E3** (a single organisational announcement, uncorroborated preprint, registry entry, or otherwise inadequately checked claim). E1 does not automatically mean journal refereeing. E3 is used when successful compilation or an exact check is merely reported without a version-specific corroborated build record, including all single-source organisational reports. A report of Lean use alone is insufficient. No E2 row met this stricter documentary threshold in the present audit; E3 does not imply that a claim is false. The separate **engineering link** grades are **D** (theorem directly gives an applicable engineering inequality), **M** (mathematical objects and the engineering problem correspond structurally, but a design algorithm is required), **H** (testable hypothesis without a direct transfer theorem), and **R** (remote analogy). Grades are neither an impact ranking nor proof of usefulness.

The 51 rows represent **49 named target families** after consolidating two pairs of separately listed subparts: Erdős #12(i)/(ii) and #741(i)/(ii). The ten grouped advances in the OpenAI August 2026 announcement appear in *eleven catalogue rows* because its tenth theme includes two distinct Erdős problems (#146 and #180). Thus there is no claim of eleven independent report themes. The earlier 37/5/9 single-axis counting has been withdrawn; all reported mathematical outcomes must be interpreted through the two-axis coding and original proof statements. In the current 51-row audit, the result-type totals are 27 P, 9 X, 9 B and 6 K, while the evidence grades are 6 E1, 0 E2 and 45 E3. These are editorial evidence labels, not independent proof-verification counts; the full row-by-row source audit is supplied as a CSV.

2.3. Non-Examples and Selection Bias

Proficiency in mathematical olympiads does not by itself resolve an open research question. Nor should unreviewed purported solutions of the Riemann hypothesis, global Navier–Stokes regularity, the unrestricted Unique Games conjecture, the Yang–Mills mass gap or an entire century-old theory be counted without comprehensive independent review. Claims about a counterexample may settle a multi-dimensional version while leaving an important two-dimensional case open; the catalogue states such restrictions. The selection intentionally includes formal-target resolutions, record constructions and bounds to show *how* AI contributes; therefore its total is a count of selected mathematical findings, not an exhaustive count of solved worldwide problems.

3. Anatomy of an AI-Assisted Mathematical Solution

3.1. Five Discovery Modes and a Five-Stage Workflow

The five *workflow stages* are conjecture encoding, candidate generation, deterministic validation, mathematical exposition, and downstream translation. These are distinct from the following five *discovery modes*. In the **formal proof search** pathway, a model proposes proof tactics or intermediate statements, a proof assistant type-checks them against explicitly stated axioms, and an independently inspectable theorem statement becomes the result. In **human–AI proof development**, models propose lemmas and mathematicians repair hypotheses and supply a conventional argument. In **constructive discovery**, search generates a graph, polynomial, matrix or configuration, which is verified by exact arithmetic or computer algebra. In **counterexample discovery**, a finite object falsifies a universal claim, with an exact test for each relevant property. Finally, **bound improvement** produces a new inequality, complexity exponent or feasible design that improves a best-known benchmark but may leave the ultimate conjecture unresolved [1,2,9,10].

© 2026 by the author(s). Distributed under a Creative Commons CC BY license.

Preprints.org | NOT PEER-REVIEWED | Posted: 23 November 2026 https://doi.org/10.20944/preprints202611.2339.v1

For an algorithmically verified certificate c and mathematical assertion Q, one may view the workflow as

$$c \leftarrow \mathcal{S}_{\mathrm{AI}}(Q, \mathcal{D}), \qquad \mathsf{Check}_{\mathrm{exact}}(Q, c) = \mathsf{true}, \tag{1}$$

where $\mathcal{D}$ contains earlier papers and proof-library facts. The checker, not the generative language model, is the decisive formal-evidence layer. Engineering transfer requires a *second* certificate for a domain model, constraints, and performance metric; the correctness of Q does not certify the engineering model.

3.2. A Theorem-to-Engineering Traceability Chain

For reproducibility, each proposed application should document: (1) the theorem and hypotheses; (2) a domain-specific mapping between mathematical and engineering variables; (3) assumptions about measurement noise, finite precision, topology or uncertainty; (4) the new algorithm, inequality or design constraint; (5) a relevant baseline; (6) a falsifiable hypothesis; and (7) independent verification. The following detailed catalogue uses the short format *background–proof and AI role–engineering transfer*. Its bracketed source is a starting point for checking the original theorem, not a substitute for specialist mathematical scrutiny.

4. Expanded Catalogue of 51 AI-Assisted Mathematical Findings

The catalogue covers 51 selected findings, not 51 distinct conjectures conclusively resolved. They include distinct formal targets, precise special-case solutions, and improvements to still-open questions. Every entry identifies the original mathematical issue, the AI-assisted contribution and the engineering opportunity. In Tables 1–3, Type and evidence are separate axes as defined in Section 2.2; a reported proof does not establish peer-reviewed acceptance.

Table 1. AI-assisted mathematics and engineering translation, cases 1–17. Type P=proof, X=counterexample, B=bound, K=construction; evidence E1=independent written review/peer-reviewed, E2=corroborated version-specific formal check, E3=lower verification; D/M/H/R are engineering links.

#	Mathematical target (year)	T.	Evid.	Link	Area	Potential engineering direction
1	Erdős #848: squarefree avoidance (2025)	P	E3	H	number theory	Modular constraints can inform discrete scheduling codes and arithmetic test-vector construction, but no direct electrical-performance theorem follows.
2	FunSearch cap-set constructions (2024)	B	E1	H	additive combinatorics	Three-term-progression-free sequences motivate interference-aware codebooks and resource allocation, subject to a new physical interference model.
3	AlphaEvolve 4-by-4 matrix multiplication (2025)	K	E3	H	algebraic algorithms	Specialised DSP, FPGA linear-algebra kernels and transformer accelerators may benefit after numerical error and overhead are measured.
4	AlphaEvolve kissing configuration in dimension 11 (2025)	K	E3	H	discrete geometry	Geometric packing provides candidate codebook or waveform configurations; physical distance metrics must be separately defined.
5	Erdős #728: factorial-divisibility gap (2026)	P	E3	H	number theory	Proof search around modular arithmetic could strengthen scheduling, arithmetic-coded test patterns, and digital design verification, but the theorem itself is not a coding gain.

© 2026 by the author(s). Distributed under a Creative Commons CC BY license.

Preprints.org | NOT PEER-REVIEWED | Posted: 23 November 2026 https://doi.org/10.20944/preprints202611.2339.v1

Table 1 continued from previous page

#	Mathematical target (year)	T.	Evid.	Link	Area	Potential engineering direction
6	Erdős #729: factorial quotient and small primes (2026)	P	E3	H	number theory	A possible role is constructing modular-robust integer constraints for exact electronic computation; practical utility remains speculative.
7	Erdős #652: planar distance incidences (2026)	P	E3	H	discrete geometry	Sensor deployment and range-only localisation are analogues, not consequences; a suitable incidence objective must first be derived.
8	Erdős #1051: irrational fast series (2026)	P	E3	R	Diophantine approximation	Irrational sampling and frequency synthesis may use Diophantine methods, but the solved series theorem has no immediate oscillator-design corollary.
9	Fel conjecture on numerical-semigroup syzygies (2026)	P	E3	H	commutative algebra	Numerical-semigroup representability appears in production scheduling and integer-resource allocation, potentially motivating new optimisation constraints.
10	Erdős planar unit-distance conjecture (2026)	X	E1	H	discrete geometry	Dense equal-range geometric structures may inspire localisation stress tests and antenna-placement benchmarks, not automatic physically realisable layouts.
11	Borsuk counterexample in dimension 63 (2026)	K	E3	H	geometry	High-dimensional clustering and metric-embedding stress tests could adopt the construction to test partition heuristics.
12	Cycle double cover conjecture (2026)	P	E1	H	graph theory	CDC may guide cycle-set enumeration; fast p-cycle protection already existed independently of the theorem.
13	Jacobian conjecture in dimensions at least three (2026)	X	E3	H	algebraic geometry	Global inverse ambiguity is classical in real sensing; evaluate a projection-LMI design instead.
14	Crouzeix sharp numerical-range conjecture (2026)	P	E3	H	matrix analysis	General polynomial-response matrix bounds motivate controller and signal-processing tests; monomial powers were bounded classically by Berger.
15	Sendov critical-point conjecture (2026)	P	E3	H	complex analysis	May motivate pole geometry and finite-word-length filter robustness studies, but it does not already bound coefficient sensitivity.
16	Existence of non-sofic groups (2026)	K	E3	R	group theory	Mostly a theoretical limitation on finite approximations, with remote analogies to verification and distributed state machines.
17	Connes rigidity conjecture (2026)	X	E3	R	operator algebras	Possible long-term relevance to quantum information/operator models, not a ready signal-processing design rule.

© 2026 by the author(s). Distributed under a Creative Commons CC BY license.

Preprints.org | NOT PEER-REVIEWED | Posted: 23 November 2026 https://doi.org/10.20944/preprints202611.2339.v1

Table 2. AI-assisted mathematics and engineering translation, cases 18–34. Type P=proof, X=counterexample, B=bound, K=construction; evidence E1=independent written review/peer-reviewed, E2=corroborated version-specific formal check, E3=lower verification; D/M/H/R are engineering links.

#	Mathematical target (year)	T.	Evid.	Link	Area	Potential engineering direction
18	Ehrhart volume conjecture (2026)	P	E3	H	convex geometry	Suggests geometry-aware integer relaxation analysis for power dispatch and lattice quantisation, pending application-specific bounds.
19	Approximate closest-vector hardness (2026)	P	E3	H	complexity theory	A reported $n^{1/400}$ hardness factor for Euclidean GapCVP, not a new finite-alphabet MIMO decoder.
20	Erdős #183: multicolour triangle Ramsey growth (2026)	B	E3	H	Ramsey theory	Potentially supplies extremal test patterns for channel colouring and interference assignment, but physical channel constraints differ.
21	Erdős #146: extremal degeneracy (2026)	X	E3	R	extremal graph theory	Indirect use in certifying network-family constraints; does not automatically establish feeder reliability.
22	Erdős #180: extremal compactness (2026)	X	E3	H	extremal graph theory	Possible sparse-topology design and graph algorithm benchmark; real network conditions need additional constraints.
23	Köthe nil-ideal conjecture (2026)	X	E3	R	ring theory	Remote conceptual relevance to symbolic algebra, exact matrix structures, and theorem-driven computer algebra verification.
24	Erdős–Sós tree embedding (#548) (2026)	P	E1	H	graph theory	Tree-embedding theorems can benchmark multicast monitoring, spanning communication design and distributed grid control.
25	Erdős #571: rational Turán exponents (2026)	P	E3	H	extremal graph theory	Suggests graph-density scaling examples for resilient network layouts; no direct electrical scaling guarantee.
26	Erdős #126: prime factors in pairwise sums (2026)	P	E3	H	additive number theory	Potential arithmetic sequence design for multiplexed systems, with no demonstrated communications advantage.
27	Erdős #74: locally almost-bipartite graphs (2026)	X	E3	H	graph theory	Relevant as a cautionary test instance for distributed graph colouring and resource assignment.
28	Erdős #1: distinct subset sums (2026)	X	E3	H	additive combinatorics	Could inspire collision-free integer signatures; energy or spectral cost may erase the combinatorial advantage.
29	Erdős #12(i): dense divisibility-free sets (2026)	P	E3	H	additive number theory	Potential building block for exact integer event scheduling under modular conflicts.
30	Erdős #12(ii): near-dense divisibility-free sets (2026)	P	E3	H	additive number theory	Could influence constructive resource assignment with forbidden arithmetic relations, following application-specific proofs.
31	Erdős #125: mixed-base sparse sumsets (2026)	P	E3	H	additive combinatorics	A possible tool for mixed-radix sensing codes and sparse integer spectrum occupancy; adaptation must be demonstrated.

Continued on next page

© 2026 by the author(s). Distributed under a Creative Commons CC BY license.

Preprints.org | NOT PEER-REVIEWED | Posted: 23 November 2026 https://doi.org/10.20944/preprints202611.2339.v1

Table 2 continued from previous page

#	Mathematical target (year)	T.	Evid.	Link	Area	Potential engineering direction
32	Erdős #138: van der Waerden gap variant (2026)	P	E3	H	Ramsey theory	Suggests tests for finite sequence colouring in medium-access scheduling; not a guarantee of RF capacity.
33	Erdős #152: isolated sumset points (2026)	P	E3	H	additive combinatorics	Potential structure for low-collision frequency hopping or coded aperture patterns, with a revised hardware objective.
34	Erdős #741(i): sumset-density partition (2026)	P	E3	H	additive number theory	Possible resource splitting for two interference channels; sumset density is only a surrogate for real packet success.

Table 3. AI-assisted mathematics and engineering translation, cases 35–51. Type P=proof, X=counterexample, B=bound, K=construction; evidence E1=independent written review/peer-reviewed, E2=corroborated version-specific formal check, E3=lower verification; D/M/H/R are engineering links.

#	Mathematical target (year)	T.	Evid.	Link	Area	Potential engineering direction
35	Erdős #741(ii): bounded-gap additive basis (2026)	P	E3	H	additive number theory	Possible combinatorial resilience test vectors for independent transmitters or energy dispatch scheduling.
36	Erdős #846: general-position decomposition (2026)	X	E3	H	discrete geometry	Cautionary examples for geometric sensor-subset decomposition and localisation scheduling.
37	Erdős #26: shifted multiples variant (2026)	P	E3	H	additive number theory	Suggests exact modular exclusion tests for integer schedules; does not directly give an efficient implementation.
38	Zanello pure-O-sequence log concavity (2026)	P	E3	H	commutative algebra	Could influence coefficient-shape constraints for polynomial approximations, though no established electronic circuit benefit follows.
39	Graffiti spanning-tree leaf conjecture (2026)	P	E3	H	graph combinatorics	Direct potential in sensor aggregation trees and topology heuristics, where energy, edge costs and reliability must be included.
40	Anchored gradient descent-ascent rate (2026)	B	E3	D	optimisation	Direct candidate for convex-concave surrogate design of robust power-electronics and communication-control optimisers.
41	OEIS A051293 subset-integer averages (2026)	P	E3	R	analytic combinatorics	Related root-of-unity filters arise in OFDM arithmetic, coding and modular FFT tests, though the exact OEIS result is indirect.
42	Balabdaoui-Wellner Chernoff-density conjecture (2026)	P	E3	H	probability	Statistical uncertainty quantification in change-point estimation and sensor calibration may exploit log-concave posterior approximations.
43	Twelve new Hadamard orders below 2000 (2026)	K	E1	M	orthogonal designs	Verified explicit orders enable exact orthogonal patterns; benefit over padded Walsh patterns requires hardware tests.
44	Complex matrix multiplication exponent at most 9/4 (2026)	B	E1	M	algorithms	Arithmetic-operation exponent over $\mathbb{C}$; practical matrix products still require finite precision and hardware tests.

Continued on next page

© 2026 by the author(s). Distributed under a Creative Commons CC BY license.

Preprints.org | NOT PEER-REVIEWED | Posted: 23 November 2026 https://doi.org/10.20944/preprints202611.2339.v1

Table 3 continued from previous page

#	Mathematical target (year)	T.	Evid.	Link	Area	Potential engineering direction
45	Subquadratic 3SUM hypothesis refutation (2026)	B	E3	H	complexity algorithms	Algorithmic geometry and collision detection may eventually benefit; theoretical exponent reductions need not beat conventional implementations.
46	Subcubic APSP hypothesis refutation (2026)	B	E3	H	complexity algorithms	Network routing, restoration planning and digital-twin topology diagnostics are conceivable consumers at sufficiently large scales.
47	Quantum parallel repetition (2026)	P	E3	R	quantum information	Conceptual value for quantum communication security and device-independent tests; engineering protocols require additional assumptions.
48	High-dimensional sphere-packing upper bounds (2026)	B	E3	H	geometry	Upper limits constrain Euclidean codebooks and signal constellations but are not recipes for constructing them.
49	Binary and spherical code upper bounds (2026)	B	E3	H	coding theory	Use for asymptotic feasibility checks in 6G, storage coding and constellation optimisation.
50	Restricted arithmetic permanent formula lower bounds (2026)	B	E3	R	algebraic complexity	A restricted arithmetic-formula bound $n^4 / \log n$ is not a general arithmetic-circuit lower bound.
51	Record high-rank elliptic curves (2026)	K	E3	R	number theory	Possible long-term algebraic-cryptography background; high-rank curves are not an automatic security improvement.

4.1. Individual Mathematical Backgrounds, AI Evidence and Transfer Limits

Cases are numbered identically to Tables 1–3. The two axes in each case header refer to the result type (P/X/B/K) and the evidence level (E1/E2/E3) in Section 2.2; a result is not considered settled merely because a formal artefact is linked.

Case 01: Erdős #848: squarefree avoidance. *Type P, evidence E3. Mathematical background:* Erdős and Sárközy asked for the largest integer subset for which every product ab+1 fails to be squarefree. *Result and AI contribution:* Sawhney and collaborators, with a key GPT-generated idea, proved the extremal residue-class answer for sufficiently large N; the original all-N claim needs separate finite treatment. *Engineering opportunity and boundary:* Modular constraints can inform discrete scheduling codes and arithmetic test-vector construction, but no direct electrical-performance theorem follows. [11].

Case 02: FunSearch cap-set constructions. *Type B, evidence E1. Mathematical background:* A cap set in a finite vector space contains no three distinct points in an arithmetic progression; its exact maximum in general dimension remains unknown. *Result and AI contribution:* LLM-guided evolutionary program search found improved lower-bound constructions, evaluated by exact combinatorial tests; it did not solve the cap-set problem. *Engineering opportunity and boundary:* Three-term-progression-free sequences motivate interference-aware codebooks and resource allocation, subject to a new physical interference model. [2].

Case 03: AlphaEvolve 4-by-4 matrix multiplication. *Type K, evidence E3. Mathematical background:* The tensor rank of small matrix multiplication measures the minimal scalar products required for a bilinear multiplication scheme. *Result and AI contribution:* AlphaEvolve reported a rank-48 algorithm for 4-by-4 multiplication over the complex numbers; real/binary arithmetic and hardware transfer require separate analysis, an improvement for this fixed computational task rather than a solution of the general rank problem. *Engineering opportunity and boundary:* Specialised DSP, FPGA linear-algebra

© 2026 by the author(s). Distributed under a Creative Commons CC BY license.

Preprints.org | NOT PEER-REVIEWED | Posted: 23 November 2026 https://doi.org/10.20944/preprints202611.2339.v1

kernels and transformer accelerators may benefit after numerical error and overhead are measured. [9].

Case 04: AlphaEvolve kissing configuration in dimension 11. *Type K, evidence E3. Mathematical background:* Kissing-number problems ask how many equal spheres may simultaneously touch another sphere without overlapping. *Result and AI contribution:* Search found an improved high-dimensional construction, a new lower bound; the exact kissing number for dimension 11 was not settled. *Engineering opportunity and boundary:* Geometric packing provides candidate codebook or waveform configurations; physical distance metrics must be separately defined. [12].

Case 05: Erdős #728: factorial-divisibility gap. *Type P, evidence E3. Mathematical background:* The old question asks whether factorial products can exhibit controlled logarithmic divisibility gaps for infinitely many integer triples. *Result and AI contribution:* GPT-5.2 Pro and Aristotle generated a Lean-checked argument; Sothanaphan reconstructed it through binomial divisibility, prime-adic valuations and base-p carries. *Engineering opportunity and boundary:* Proof search around modular arithmetic could strengthen scheduling, arithmetic-coded test patterns, and digital design verification, but the theorem itself is not a coding gain. [13].

Case 06: Erdős #729: factorial quotient and small primes. *Type P, evidence E3. Mathematical background:* This companion question asks whether denominators of factorial quotients may be supported on bounded primes even beyond a logarithmic parameter gap. *Result and AI contribution:* The problem registry reports an affirmative result with AI/Lean assistance, adapting ideas from #728. This registry citation is not a primary proof publication and is insufficient for precise author attribution. *Engineering opportunity and boundary:* A possible role is constructing modular-robust integer constraints for exact electronic computation; practical utility remains speculative. [14].

Case 07: Erdős #652: planar distance incidences. *Type P, evidence E3. Mathematical background:* Erdős #652 concerns extremal point-distance configurations, connecting rich and sparse incidence structures in the plane. *Result and AI contribution:* Aletheia produced a reduction to existing incidence bounds; human authors corrected misquoted exponents. The result is logically valid but inherits mathematics in the literature. *Engineering opportunity and boundary:* Sensor deployment and range-only localisation are analogues, not consequences; a suitable incidence objective must first be derived. [10].

Case 08: Erdős #1051: irrational fast series. *Type P, evidence E3. Mathematical background:* The Erdős–Graham problem asks for irrationality of rapidly convergent series under arithmetic growth hypotheses. *Result and AI contribution:* Aletheia supplied a proof using tail estimates and a Mahler-style criterion; authors corrected a minor strict-inequality issue and proved broader results with human collaboration. *Engineering opportunity and boundary:* Irrational sampling and frequency synthesis may use Diophantine methods, but the solved series theorem has no immediate oscillator-design corollary. [10].

Case 09: Fel conjecture on numerical-semigroup syzygies. *Type P, evidence E3. Mathematical background:* Fel predicted a universal formula expressing normalised syzygy invariants of numerical semigroups from gap sums and symmetric polynomials. *Result and AI contribution:* Axiom Prover built an autonomous Lean/Mathlib proof from natural-language definitions, via exponential generating functions and Hilbert-series identities. *Engineering opportunity and boundary:* Numerical-semigroup representability appears in production scheduling and integer-resource allocation, potentially motivating new optimisation constraints. [15].

Case 10: Erdős planar unit-distance conjecture. *Type X, evidence E1. Mathematical background:* Erdős conjectured that among n planar points the maximal number of unit-distance pairs is n to the power 1+o(1). *Result and AI contribution:* An AI-generated algebraic-number-theoretic construction yields at least n to the power 1+delta along infinitely many n; external mathematicians published an independent exposition. *Engineering opportunity and boundary:* Dense equal-range geometric structures may inspire localisation stress tests and antenna-placement benchmarks, not automatic physically realisable layouts. [16].

© 2026 by the author(s). Distributed under a Creative Commons CC BY license.

Preprints.org | NOT PEER-REVIEWED | Posted: 23 November 2026 https://doi.org/10.20944/preprints202611.2339.v1

Case 11: Borsuk counterexample in dimension 63. *Type K, evidence E3. Mathematical background:* Borsuk conjectured that any bounded n-dimensional set could be partitioned into n+1 smaller-diameter parts; this was already refuted in high dimensions. *Result and AI contribution:* Max Grinsztajn is credited with a 321-point construction in dimension 63; Nicholas Konz's project page reports rediscovery and a separate exact-arithmetic certificate. Yibo Ji also describes the construction in an arXiv preprint. These are non-peer-reviewed sources; the original verifier was not run here. *Engineering opportunity and boundary:* High-dimensional clustering and metric-embedding stress tests could adopt the construction to test partition heuristics. [17,18].

Case 12: Cycle double cover conjecture. *Type P, evidence E1. Mathematical background:* Szekeres and Seymour conjectured that each bridgeless finite graph possesses a multiset of cycles covering each edge exactly twice. *Result and AI contribution:* A 2026 AI-generated proof claim prompted independent expositions by Geelen and Oum; as with any major claim, longer-form refereeing remains separate from those expositions. The claimed conclusion is a combinatorial existence statement, not a routing guarantee. *Engineering opportunity and boundary:* Strong analogy to survivable IoT backbones and substation communication; cycle allocation and latency/physical fault constraints require new optimisation. [6].

Case 13: Jacobian conjecture in dimensions at least three. *Type X, evidence E3. Mathematical background:* The original conjecture says a polynomial map over complex numbers with nonzero constant Jacobian determinant must have a polynomial inverse. *Result and AI contribution:* A 2026 AI-assisted preprint constructs noninjective polynomial maps countering the claim for every dimension at least three; Gao gives symbolic verification details and generalisations. The complex planar case remains a separate question; this article does not certify the preprint claim. *Engineering opportunity and boundary:* Critical warning for nonlinear sensor calibration and power-system digital-twin inversion: local full rank alone does not establish global identifiability. [19].

Case 14: Crouzeix sharp numerical-range conjecture. *Type P, evidence E3. Mathematical background:* For decades the sharp universal spectral-set constant for polynomial functions of a nonnormal matrix was unknown. *Result and AI contribution:* A 2026 preprint by Jin reports a proof of the inequality $\|p(A)\| \leq 2 \max_{z \in \mathcal{W}(A)} |p(z)|$, with a central AI-generated argument; Townsend and Greenbaum reported expert checking (including Crouzeix) in SIAM News, not a stand-alone detailed proof verification or journal-refereed proof; E3 is assigned conservatively. Independently of the sharp constant, the 2017 Crouzeix–Palencia constant already suffices for the engineering developments in Section 5. *Engineering opportunity and boundary:* The general polynomial-function inequality motivates output-response and filter certification; classical Berger bounds already apply to matrix powers. [3].

Case 15: Sendov critical-point conjecture. *Type P, evidence E3. Mathematical background:* If all roots of a polynomial lie in the unit disk, Sendov predicted each root has a critical point of the polynomial within unit distance. *Result and AI contribution:* Tao's August 2026 mathematical blog reports an all-degree Lean-verified proof by Lech Mazur and provides an exposition. This cited blog is not a peer-reviewed article; a pinned successful build was not independently verified. *Engineering opportunity and boundary:* May motivate pole geometry and finite-word-length filter robustness studies, but it does not already bound coefficient sensitivity. [20].

Case 16: Existence of non-sofic groups. *Type K, evidence E3. Mathematical background:* The sofic-group question asked whether every group admits finite approximate permutation models. *Result and AI contribution:* OpenAI reported a construction of a non-sofic group together with a formal-certificate claim; specialist uptake and longer-form algebraic vetting remain separate from the certificate report. *Engineering opportunity and boundary:* Mostly a theoretical limitation on finite approximations, with remote analogies to verification and distributed state machines. [21].

Case 17: Connes rigidity conjecture. *Type X, evidence E3. Mathematical background:* A rigidity conjecture proposed uniqueness properties of groups reconstructed from associated von Neumann algebras.

© 2026 by the author(s). Distributed under a Creative Commons CC BY license.

Preprints.org | NOT PEER-REVIEWED | Posted: 23 November 2026 https://doi.org/10.20944/preprints202611.2339.v1

Result and AI contribution: An AI-generated counterexample and reported formal certificate were released against the stated rigidity property; this catalogue records the report while recognising that later mathematical vetting may further clarify the claim. *Engineering opportunity and boundary:* Possible long-term relevance to quantum information/operator models, not a ready signal-processing design rule. [21].

Case 18: Ehrhart volume conjecture. *Type P, evidence E3. Mathematical background:* The conjecture concerns maximal volume of a convex body whose centroid is its only interior lattice point. *Result and AI contribution:* The 2026 AI contribution reported a dimension-uniform extremal characterisation with a Lean certificate. *Engineering opportunity and boundary:* Suggests geometry-aware integer relaxation analysis for power dispatch and lattice quantisation, pending application-specific bounds. [21].

Case 19: Approximate closest-vector hardness. *Type P, evidence E3. Mathematical background:* Closest vector asks for a lattice point near a prescribed target; approximation hardness in Euclidean norm was incompletely understood. *Result and AI contribution:* The 2026 OpenAI report claims NP-hardness of Euclidean GapCVP$_{n^{1/400}}$ under polynomial-time reductions from 3-SAT, where n is lattice rank; a Lean proof artefact was reported but was not independently compiled in this study. The result is about a worst-case promise problem, not finite-alphabet MIMO BER. *Engineering opportunity and boundary:* Constrains worst-case promises for MIMO lattice decoding and lattice cryptography; it does not itself accelerate a receiver. [21].

Case 20: Erdős #183: multicolour triangle Ramsey growth. *Type B, evidence E3. Mathematical background:* The multicolour Ramsey question asks how large complete graphs can be coloured without a monochromatic triangle. *Result and AI contribution:* The 2026 AI argument supplied a superexponential lower-bound construction resolving the stated Erdős problem. *Engineering opportunity and boundary:* Potentially supplies extremal test patterns for channel colouring and interference assignment, but physical channel constraints differ. [21].

Case 21: Erdős #146 (degeneracy conjecture). *Type X, evidence E3. Mathematical background:* For every bipartite r-degenerate forbidden graph H, the conjecture proposed $\mathrm{ex}(n, H) = O(n^{2-1/r})$. *Reported AI result:* A 2026 OpenAI report describes an explicit bipartite 2-degenerate counterexample exceeding the predicted exponent; the linked Lean artefact has not been compiled in this study. *Engineering limit:* The result does not by itself improve topology design. [21].

Case 22: Erdős #180 (extremal compactness). *Type X, evidence E3. Mathematical background:* For a finite family of forbidden graphs, does the joint extremal number compare in order to some single member's extremal number? *Reported AI result:* A reported 2026 connected bipartite cyclic-family counterexample addresses a strengthened version; earlier elementary star–matching examples already disprove an unrestricted reading. *Engineering limit:* The result is not a restoration algorithm. [21].

Case 23: Köthe nil-ideal conjecture. *Type X, evidence E3. Mathematical background:* Köthe asked whether the sum of two nil left ideals of an arbitrary ring must always be nil. *Result and AI contribution:* Adamczewski, Böhmler and Marczinzik reported an AI-assisted counterexample accompanied by algebraic proof material that can be independently checked. *Engineering opportunity and boundary:* Remote conceptual relevance to symbolic algebra, exact matrix structures, and theorem-driven computer algebra verification. [22].

Case 24: Erdős–Sós tree embedding (#548). *Type P, evidence E1. Mathematical background:* The conjecture states that every graph with more than (k-2)n/2 edges contains every tree on k vertices, in the appropriate size range. *Result and AI contribution:* An AI-assisted proof was reported; Riordan and Scott subsequently supplied a shorter human-written proof in a 2026 preprint. The result should be interpreted according to its exact hypotheses and independently reviewed proof text. *Engineering opportunity and boundary:* Tree-embedding theorems can benchmark multicast monitoring, spanning communication design and distributed grid control. [23].

© 2026 by the author(s). Distributed under a Creative Commons CC BY license.

Preprints.org | NOT PEER-REVIEWED | Posted: 23 November 2026 https://doi.org/10.20944/preprints202611.2339.v1

Case 25: Erdős #571: rational Turán exponents. *Type P, evidence E3. Mathematical background:* The rational-exponents problem asks whether each rational r between 1 and 2 is realised as an extremal exponent for a forbidden bipartite graph. *Result and AI contribution:* An AI-assisted argument for the stated rational range is described in the cited Adamczewski–Bloom preprint; the specific formal statement and proof environment were not independently recompiled here. *Engineering opportunity and boundary:* Suggests graph-density scaling examples for resilient network layouts; no direct electrical scaling guarantee. [24].

Case 26: Erdős #126: prime factors in pairwise sums. *Type P, evidence E3. Mathematical background:* Erdős asked for growth of the number of distinct prime factors arising in pairwise sums of suitably chosen integer sets. *Result and AI contribution:* A formal agent gave a lower bound considerably stronger than the logarithmic target, with a reported proof check; a corroborated build was not established here. *Engineering opportunity and boundary:* Potential arithmetic sequence design for multiplexed systems, with no demonstrated communications advantage. [24].

Case 27: Erdős #74: locally almost-bipartite graphs. *Type X, evidence E3. Mathematical background:* A local-to-global colouring conjecture asked whether arbitrarily slow edge-deletion corrections could prevent global 3-colourability. *Result and AI contribution:* The source reports a formal counterexample to the proposed obstruction; a corroborated build was not available in this audit. *Engineering opportunity and boundary:* Relevant as a cautionary test instance for distributed graph colouring and resource assignment. [24].

Case 28: Erdős #1: distinct subset sums. *Type X, evidence E3. Mathematical background:* Erdős proposed an exponential lower threshold for the largest element in sets with all subset sums distinct. *Result and AI contribution:* An AI-generated lattice construction is reported to refute the conjectured absolute constant, reported as formally checked, with an ineffective asymptotic dimension threshold and no corroborated build in this audit. *Engineering opportunity and boundary:* Could inspire collision-free integer signatures; energy or spectral cost may erase the combinatorial advantage. [24].

Case 29: Erdős #12(i): dense divisibility-free sets. *Type P, evidence E3. Mathematical background:* Erdős and Sárközy sought large infinite integer sets without an element dividing the sum of two larger ones. *Result and AI contribution:* The formal-proof-search work used block constructions, the Chinese remainder theorem and progression-free subsets; the result has a Lean proof. *Engineering opportunity and boundary:* Potential building block for exact integer event scheduling under modular conflicts. [1].

Case 30: Erdős #12(ii): near-dense divisibility-free sets. *Type P, evidence E3. Mathematical background:* This stronger asymptotic version asks how dense such a divisibility-constrained infinite set can be. *Result and AI contribution:* A separate formal construction using CRT and Behrend-type progression-free layers gives growth above N to the power 1-epsilon. *Engineering opportunity and boundary:* Could influence constructive resource assignment with forbidden arithmetic relations, following application-specific proofs. [1].

Case 31: Erdős #125: mixed-base sparse sumsets. *Type P, evidence E3. Mathematical background:* Whether the sum of base-3 and base-4 missing-digit sets has positive lower density was unresolved. *Result and AI contribution:* Formal proof search supplied a thinning argument exploiting near coincidences between powers of 3 and 4 and proves lower density zero. *Engineering opportunity and boundary:* A possible tool for mixed-radix sensing codes and sparse integer spectrum occupancy; adaptation must be demonstrated. [1].

Case 32: Erdős #138: van der Waerden gap variant. *Type P, evidence E3. Mathematical background:* This variant concerns the asymptotic difference between consecutive two-colour van der Waerden numbers. *Result and AI contribution:* An autonomous Lean proof established the specified variant using a colouring-extension argument. *Engineering opportunity and boundary:* Suggests tests for finite sequence colouring in medium-access scheduling; not a guarantee of RF capacity. [1].

© 2026 by the author(s). Distributed under a Creative Commons CC BY license.

Preprints.org | NOT PEER-REVIEWED | Posted: 23 November 2026 https://doi.org/10.20944/preprints202611.2339.v1

Case 33: Erdős #152: isolated sumset points. *Type P, evidence E3. Mathematical background:* The question asks whether sufficiently large Sidon sets force many isolated elements of their pairwise sumset. *Result and AI contribution:* An AI-discovered combinatorial counting proof was formalised, comparing shifted neighbours and quadruples. *Engineering opportunity and boundary:* Potential structure for low-collision frequency hopping or coded aperture patterns, with a revised hardware objective. [1].

Case 34: Erdős #741(i): sumset-density partition. *Type P, evidence E3. Mathematical background:* This multipart question asks about splitting a set while preserving positive upper density in each partial sumset. *Result and AI contribution:* The specified first part was solved by formal case analysis and density inequalities. *Engineering opportunity and boundary:* Possible resource splitting for two interference channels; sumset density is only a surrogate for real packet success. [1].

Case 35: Erdős #741(ii): bounded-gap additive basis. *Type P, evidence E3. Mathematical background:* A second part asks for a specially constructed additive basis robust under arbitrary two-way partitions. *Result and AI contribution:* The agent gave a rapidly growing explicit construction and Lean proof for the precise multipart target. *Engineering opportunity and boundary:* Possible combinatorial resilience test vectors for independent transmitters or energy dispatch scheduling. [1].

Case 36: Erdős #846: general-position decomposition. *Type X, evidence E3. Mathematical background:* Erdős asked if an infinite planar set with many general-position points in each finite subset must split into finitely many general-position sets. *Result and AI contribution:* An AI-generated construction maps edges of an infinite complete graph to planar points, thereby refuting the finite-decomposition claim. *Engineering opportunity and boundary:* Cautionary examples for geometric sensor-subset decomposition and localisation scheduling. [1].

Case 37: Erdős #26: shifted multiples variant. *Type P, evidence E3. Mathematical background:* A strengthened version of a classical shifted-multiples density question asks for a sequence with divergent reciprocal sum but uniformly sparse shifted multiples. *Result and AI contribution:* The system found a block-and-prime CRT construction proving the more general variant in Lean. *Engineering opportunity and boundary:* Suggests exact modular exclusion tests for integer schedules; does not directly give an efficient implementation. [1].

Case 38: Zanello pure-O-sequence log concavity. *Type P, evidence E3. Mathematical background:* Zanello conjectured log-concavity for pure O-sequences of codimension three and type two, a gap left by prior unimodality results. *Result and AI contribution:* An autonomous proof converted Hilbert-function counting into explicit inequalities and case distinctions, formally checked. *Engineering opportunity and boundary:* Could influence coefficient-shape constraints for polynomial approximations, though no established electronic circuit benefit follows. [1].

Case 39: Graffiti spanning-tree leaf conjecture. *Type P, evidence E3. Mathematical background:* A 1996 automated-conjecturing problem relates the maximum number of leaves of a spanning tree to local neighbourhood independent sets. *Result and AI contribution:* The formal-proof-search study reported a proof of the bound through a bipartite incidence count and a spanning-tree construction. *Engineering opportunity and boundary:* Direct potential in sensor aggregation trees and topology heuristics, where energy, edge costs and reliability must be included. [1].

Case 40: Anchored gradient descent-ascent rate. *Type B, evidence E3. Mathematical background:* An open convergence-rate problem asked whether the anchored GDA saddle-point method admits an exact $O(1/t)$ last-iterate squared-gradient rate. *Result and AI contribution:* An AI agent jointly chose a parameter schedule and a Lean proof; Surina and collaborators give the mathematical analysis. *Engineering opportunity and boundary:* Direct candidate for convex-concave surrogate design of robust power-electronics and communication-control optimisers. [25].

Case 41: OEIS A051293 subset-integer averages. *Type P, evidence E3. Mathematical background:* An OEIS question asks for asymptotics of the number of nonempty subsets of 1,...,n having integer

© 2026 by the author(s). Distributed under a Creative Commons CC BY license.

Preprints.org | NOT PEER-REVIEWED | Posted: 23 November 2026 https://doi.org/10.20944/preprints202611.2339.v1

arithmetic mean. *Result and AI contribution:* The formal-proof-search study derived Fourier/root-of-unity coefficient bounds and a formal proof of the conjectured asymptotic formula. *Engineering opportunity and boundary:* Related root-of-unity filters arise in OFDM arithmetic, coding and modular FFT tests, though the exact OEIS result is indirect. [1].

Case 42: Balabdaoui-Wellner Chernoff-density conjecture. *Type P, evidence E3. Mathematical background:* The 2014 conjecture asserted strong log-concavity for the density of the argmax of two-sided Brownian motion minus a parabola. *Result and AI contribution:* A 2026 Zhang–Zhou preprint reports an AI-generated proof, connecting the conjecture to shape-constrained inference; specialist refereeing remains an additional step. *Engineering opportunity and boundary:* Statistical uncertainty quantification in change-point estimation and sensor calibration may exploit log-concave posterior approximations. [26].

Case 43: Twelve newly constructed Hadamard orders below 2000. *Type K, evidence E1. Mathematical background:* A Hadamard matrix H has signs +/-1 and mutually orthogonal rows; existence for every multiple of four is still an open conjecture. *Result and AI contribution:* Claude-assisted constructions covered twelve previously unknown orders below 2000, later independently verified by Egan and collaborators. *Engineering opportunity and boundary:* Direct candidate matrices for orthogonal training pilots, spread-spectrum sequences, CDMA calibration and interferometer switching. [27].

Case 44: Matrix multiplication exponent at most 9/4. *Type B, evidence E1. Mathematical background:* The classical matrix-multiplication exponent ω is the infimum arithmetic-operation exponent for multiplying dense $n \times n$ matrices over a field, here considered over $\mathbb{C}$ in the algebraic arithmetic model. *Result and AI contribution:* The 2 October 2026 OpenAI preprint reports $\omega \leq 9/4$ over the complex numbers. Pass provides a constructive proof; Lü extends the construction to arbitrary characteristic, and Amanov, van den Berg and Zuiddam give an independent written exposition valid over every field. These are preprints rather than a claim of refereed consensus. This is an asymptotic algebraic operation-count bound, not an IEEE-floating-point latency result; the exact exponent remains unknown. *Engineering opportunity and boundary:* May eventually reduce dense model-predictive-control and channel-estimation arithmetic at enormous scales, subject to constants and stability. [28–31].

Case 45: Subquadratic 3SUM hypothesis refutation. *Type B, evidence E3. Mathematical background:* The fine-grained 3SUM hypothesis asserted no truly subquadratic solution for the general benchmark problem. *Result and AI contribution:* Alman and Vassilevska Williams, with core AI-generated algorithmic ideas, give a deterministic $O(n^{1.9992})$ integer-input algorithm under their stated word model. *Engineering opportunity and boundary:* Algorithmic geometry and collision detection may eventually benefit; theoretical exponent reductions need not beat conventional implementations. [32].

Case 46: Subcubic APSP hypothesis refutation. *Type B, evidence E3. Mathematical background:* The fine-grained APSP hypothesis denies genuinely subcubic all-pairs shortest paths for weighted directed graphs. *Result and AI contribution:* The same 2026 preprint reports $O(n^{2.9995})$ for polynomially bounded integer weights under its specified model. *Engineering opportunity and boundary:* Network routing, restoration planning and digital-twin topology diagnostics are conceivable consumers at sufficiently large scales. [32].

Case 47: Quantum parallel repetition. *Type P, evidence E3. Mathematical background:* Quantum game theory lacked a general exponential parallel repetition theorem comparable to a classical theorem. *Result and AI contribution:* The OpenAI mathematics collection reports an exponential theorem for general two-player quantum games with a Lean certificate. *Engineering opportunity and boundary:* Conceptual value for quantum communication security and device-independent tests; engineering protocols require additional assumptions. [21].

Case 48: High-dimensional sphere-packing upper bounds. *Type B, evidence E3. Mathematical background:* A central density question asks for optimal packing of equal spheres in growing dimension. *Result and AI contribution:* An AI-assisted proof sharpened upper bounds toward the Cohn-Elkies

© 2026 by the author(s). Distributed under a Creative Commons CC BY license.

Preprints.org | NOT PEER-REVIEWED | Posted: 23 November 2026 https://doi.org/10.20944/preprints202611.2339.v1

threshold; exact optimal densities remain unknown. *Engineering opportunity and boundary:* Upper limits constrain Euclidean codebooks and signal constellations but are not recipes for constructing them. [21].

Case 49: Binary and spherical code upper bounds. *Type B, evidence E3. Mathematical background:* Coding-theory bounds limit how many codewords can be separated by a prescribed Hamming or Euclidean distance. *Result and AI contribution:* A model-derived argument improved high-dimensional upper bounds; the unrestricted exact code-size problem remains open. *Engineering opportunity and boundary:* Use for asymptotic feasibility checks in 6G, storage coding and constellation optimisation. [21].

Case 50: Arithmetic permanent circuit lower bounds. *Type B, evidence E3. Mathematical background:* Computing the permanent with restricted arithmetic formulas and circuits is a central algebraic complexity challenge. *Result and AI contribution:* The 2026 report states a restricted arithmetic-formula lower bound of order $n^4/\log n$, but does not solve general permanent circuit complexity. *Engineering opportunity and boundary:* Warns of complexity barriers in combinatorial sensor association or assignment enumeration. [21].

Case 51: Record high-rank elliptic curves. *Type K, evidence E3. Mathematical background:* The largest known Mordell-Weil rank of elliptic curves over the rationals is a construction record, not the solution of the unbounded-rank question. *Result and AI contribution:* AI-assisted searches reported examples of ranks at least 30 and 31, with explicit curves that can be checked. *Engineering opportunity and boundary:* Possible long-term algebraic-cryptography background; high-rank curves are not an automatic security improvement. [33].

4.2. Cross-Disciplinary Application Matrix

The following field-specific mapping uses mathematical mechanisms rather than suggestive keywords alone. "Candidate" denotes an engineering hypothesis to be built and benchmarked, not a demonstrated technology. Tables 1–3 and Table 4 are intentionally kept close to this section to prevent visual interruption of later derivations.

Table 4. Transfer pathways across engineering disciplines (proposed, not validated outcomes).

Engineering discipline	Mathematical breakthrough(s)	Candidate implementation	Required validation
Power and energy	Crouzeix; cycle double cover; Erdős–Sós	Transient bounds for inverter dynamics; communication redundancy; monitoring tree embedding	Controller baselines, feasible feeder restoration, N-1 faults
Electronics and VLSI	AlphaEvolve 4-by-4; Hadamard; matrix exponent	FPGA matrix kernels, signed calibration patterns, arithmetic complexity models	DSP slices, word length, area, energy, timing
Wireless and optical communication	CVP hardness; Hadamard; code bounds	Adaptive MIMO decoding, orthogonal training, constellation feasibility screens	BER/BLER, latency tail, channel model, power
Control and robotics	Crouzeix; anchored GDA; Jacobian counterexample	Worst-case transient certification; robust saddle-point update; inverse-kinematics injectivity	Closed-loop safety, state constraints, adversarial perturbations
Mechanical and aerospace	Closest vector; non-normal matrix bounds; graph cycles	Quantised actuator selection, aeroelastic transient bounds, sensor network survivability	Physical system identification, flutter envelopes, environmental reliability
Biomedical and medical imaging	Jacobian; Hadamard; Sendov	Identifiability of calibrated sensors, multiplexed acquisition, filter pole geometry	Phantom studies, patient-independent testing, sensitivity analysis
Civil and transportation	Graph extremal theory; 3SUM/APSP; cycle covers	Transportation fault detours and layout stress tests, sparse path computations	Capacity constraints, demand variation, real-time benchmarks

Continued on next page

© 2026 by the author(s). Distributed under a Creative Commons CC BY license.

Preprints.org | NOT PEER-REVIEWED | Posted: 23 November 2026 https://doi.org/10.20944/preprints202611.2339.v1

Table 4 continued

Engineering discipline	Mathematical breakthrough(s)	Candidate implementation	Required validation
Chemical and process engineering	Fel semigroup; Crouzeix; anchored GDA	Batch-resource schedules, nonnormal process control, robust min–max control	Mass/energy balances, process uncertainty, constraints
Quantum and computing	Connes; non-sofic groups; matrix multiplication	Operator-theoretic limitations, exact verification, accelerated numerical kernels	Noise models, gate depth, hardware scaling and proof assumption checks
Manufacturing and logistics	Erdős combinatorics; 3SUM/APSP; semigroups	Conflict-free test allocations, integer batch feasibility, faster path search	Discrete-event simulation and deployment costs

5. Electrical Engineering Translation I: Numerical-Range-Certified Converter Control

5.1. Classical Power Bounds Versus General Matrix-Function Bounds

For $F \in \mathbb{C}^{n\times n}$ write $\mathcal{W}(F) = \{v^*Fv : \|v\|_2 = 1\}$ and $w(F) = \max_{z\in\mathcal{W}(F)} |z|$. Non-normal F may have short-horizon amplification even when its spectral radius $\rho(F) < 1$ [34]. Critically, **Berger's 1965 power inequality** gives $w(F^k) \le w(F)^k$ for $k \ge 1$, while the elementary norm inequality is $\|T\|_2 \le 2w(T)$. Thus

$$\boxed{\|F^k\|_2 \le 2w(F)^k, \qquad k \ge 1.} \tag{2}$$

This is a *classical certificate*, not an AI-enabled advance [8,35]. The factor-two monomial result is not a new research hypothesis.

For a *general polynomial* $p(z) = \sum_{j=0}^{N} c_j z^j$, the published Crouzeix–Palencia theorem gives

$$\boxed{\|p(F)\|_2 \le c_{\mathrm{CP}} \max_{z\in\mathcal{W}(F)} |p(z)|, \qquad c_{\mathrm{CP}} = 1+\sqrt{2}.} \tag{3}$$

The sharper factor 2 for arbitrary polynomials is reported in a 2026 preprint and discussed in expert commentary; it is not needed here [3–5]. Unlike a coefficient-wise bound, (3) retains polynomial cancellation, but a good shifted basis may do so more effectively. For the resolvent, a stronger *elementary* result applies. For every unit v and $\zeta \notin \mathcal{W}(F)$, Cauchy–Schwarz implies $\|(\zeta I - F)v\|_2 \ge |v^*(\zeta I - F)v| \ge \operatorname{dist}(\zeta, \mathcal{W}(F))$. Inverting the minimum singular value therefore yields

$$\|(\zeta I - F)^{-1}\|_2 \le \frac{1}{\operatorname{dist}(\zeta, \mathcal{W}(F))}. \tag{4}$$

For $G(\zeta) = C(\zeta I - F)^{-1}B + D$, use $\|G(\zeta)\|_2 \le \|D\|_2 + \|C\|_2\|B\|_2 / \operatorname{dist}(\zeta, \mathcal{W}(F))$. If $w(F) < 1$, all unit-circle points lie outside the numerical range and this also bounds the discrete-time peak frequency response. The Crouzeix–Palencia constant would weaken these resolvent bounds; it is not used for this purpose.

5.2. Grid-Forming Inverter Model and Digital Sampling

A synchronised dq model of an LCL-filtered voltage-source converter may be written locally as

$$\begin{aligned}
L_f \dot{i}_{fd} &= v_{id} - v_{cd} - R_f i_{fd} + \omega L_f i_{fq},\\
L_f \dot{i}_{fq} &= v_{iq} - v_{cq} - R_f i_{fq} - \omega L_f i_{fd},\\
C_f \dot{v}_{cd} &= i_{fd} - i_{gd} + \omega C_f v_{cq},\\
C_f \dot{v}_{cq} &= i_{fq} - i_{gq} - \omega C_f v_{cd},\\
L_g \dot{i}_{gd} &= v_{cd} - v_{gd} - R_g i_{gd} + \omega L_g i_{gq},\\
L_g \dot{i}_{gq} &= v_{cq} - v_{gq} - R_g i_{gq} - \omega L_g i_{gd}.
\end{aligned} \tag{5}$$

© 2026 by the author(s). Distributed under a Creative Commons CC BY license.

Preprints.org | NOT PEER-REVIEWED | Posted: 23 November 2026 https://doi.org/10.20944/preprints202611.2339.v1

The variables are converter inductor currents i_f, filter capacitor voltages v_c, grid-side currents i_g, converter modulation voltages v_i, grid voltage v_g and reference-frame frequency ω. Droop dynamics, virtual synchronous machine states or PLL-free grid-forming phase states can be appended before linearisation. For an operating point $(x^\star, u^\star)$ and perturbations δx, δu, obtain

$$\delta \dot{x} = A_c \delta x + B_c \delta u + E_c \delta d. \tag{6}$$

Zero-order-hold sampling at T_s gives

$$\begin{aligned} A_d &= e^{A_c T_s}, & B_d &= \int_0^{T_s} e^{A_c \tau} B_c \, d\tau, \\ E_d &= \int_0^{T_s} e^{A_c \tau} E_c \, d\tau. \end{aligned} \tag{7}$$

With state feedback $\delta u_k = K \delta x_k$, the closed-loop matrix is $F(K) = A_d + B_d K$. Nonlinear saturation, modulation constraints, delays and changes in grid impedance require subsequent validation; the certificate below applies only over the stated linear or bounded-uncertainty model.

5.3. Classical Bounded-Disturbance Response with the Exact Zero-th Power

For $x_{k+1} = Fx_k + Ed_k$ with $\|d_k\|_2 \le \bar{d}$, let $\|x_0\|_2 \le \bar{x}_0$ and assume $w(F) \le \gamma < 1$. Since $\|F^0\|_2 = 1$, Berger's bound gives the sharper, *unconditional* estimate for every $k \ge 1$:

$$\boxed{\|x_k\|_2 \le 2\gamma^k \bar{x}_0 + \|E\|_2 \bar{d} \left[1 + \frac{2\gamma(1-\gamma^{k-1})}{1-\gamma} \right].} \tag{8}$$

A sufficient uniform output constraint for $z_k = Cx_k$, $k \ge 1$, is

$$\|C\|_2 \left(2\bar{x}_0 + \|E\|_2 \bar{d} \left[1 + \frac{2\gamma}{1-\gamma} \right] \right) \le I_{\max}. \tag{9}$$

For realistic controllers one must compare these bounds with direct induced norms, physical energy-coordinate Lyapunov inequalities, saturation limits, and disturbance simulations. These inequalities are not based on Crouzeix's new sharp-constant claim.

5.4. Exact Ando LMI and Robust State-Feedback Synthesis

Let $F_q(K) = A_{d,q} + B_{d,q} K$ be a fixed collection of real or complex discrete-time plant vertices (including controller delays in the model where appropriate). Ando's classical characterization establishes that $w(F_q(K)) \le \gamma$ *if and only if* a Hermitian matrix H_q exists satisfying

$$\boxed{\begin{bmatrix} \gamma I + H_q & F_q(K) \\ F_q(K)^* & \gamma I - H_q \end{bmatrix} \succeq 0.} \tag{10}$$

The constraint is jointly affine in K, H_q and γ; unlike a finite angular grid, it is exact [35,36]. One proposed convex synthesis model is

$$\begin{aligned} \min_{K,\gamma,t,\{H_q\}} \quad & \gamma + \lambda t \\ \text{s.t.} \quad & 0 \le \gamma \le 1 - \epsilon, \quad \|K\|_F \le t, \\ & \begin{bmatrix} \gamma I + H_q & F_q(K) \\ F_q(K)^* & \gamma I - H_q \end{bmatrix} \succeq 0, \ \forall q. \end{aligned} \tag{11}$$

© 2026 by the author(s). Distributed under a Creative Commons CC BY license.

Preprints.org | NOT PEER-REVIEWED | Posted: 23 November 2026 https://doi.org/10.20944/preprints202611.2339.v1

For fixed K, polytopic uncertainty is inherited without additional gridding: since $w(\cdot)$ is a norm, $w(\sum_q \alpha_q F_q(K)) \le \sum_q \alpha_q w(F_q(K)) \le \gamma$ for $\alpha_q \ge 0$ and $\sum_q \alpha_q = 1$. However, exact zero-order-hold discretization $A_d = e^{A_c T_s}$ is generally *non-affine* in uncertain physical inductances. Therefore a claim about continuous parameter variation must establish an actual matrix enclosure, not merely sample a few L_g values.

Numerical radius depends on the chosen state basis, $w(SFS^{-1}) \neq w(F)$ in general; comparisons must use a common physical energy metric or disclose the state normalization. For a Schur-stable closed-loop matrix F, a weighted Lyapunov baseline is

$$F^* P F \preceq \alpha^2 P, \quad P \succ 0 \implies \|F^k\|_2 \le \sqrt{\kappa_2(P)}\, \alpha^k. \tag{12}$$

For fixed α, common-metric state-feedback synthesis is convex after the change of variables $Y = P^{-1}$ and $Z = KY$:

$$\begin{bmatrix} \alpha^2 Y & (A_{d,q} Y + B_{d,q} Z)^T \\ A_{d,q} Y + B_{d,q} Z & Y \end{bmatrix} \succeq 0, \quad I \preceq Y \preceq tI.$$

Minimising t at fixed α bounds the metric condition number. The gain is recovered as $K = ZY^{-1}$. The original physical gain-norm constraint is not generally convex in (Y, Z); a conservative sufficient restriction is $\|Z\|_F \le b$ when $Y \succeq I$, ensuring $\|K\|_F \le b$. Section 10 implements this baseline and the exact gain-budget spectral-norm baseline.

5.5. Nonnormal Matrix and a Non-Monomial Response-Filter Example

For the synthetic transition matrix

$$F_0 = \begin{bmatrix} 0.40 & 0.35 \\ 0 & 0.40 \end{bmatrix}, \tag{13}$$

$\mathcal{W}(F_0)$ is a disk centred at 0.40 of radius 0.175, so $w(F_0) = 0.575$, $\rho(F_0) = 0.4$ and $\|F_0\|_2 = 0.611606$. For $\zeta = 1$, the exact resolvent norm is 2.2222, the elementary bound (4) is $1/0.425 = 2.35294$, and applying the Crouzeix–Palencia constant would give 5.68050. Berger already certifies the power envelope.

The following degree-two response is a *negative control*, rather than a demonstration of superiority:

$$p(z) = z^2 - 0.78z + 0.162 = (z - 0.40)^2 + 0.02(z - 0.40) + 0.01. \tag{14}$$

With $N = F_0 - 0.4I$, $N^2 = 0$, so $p(F_0) = 0.02N + 0.01I$. Its exact norm is 0.0140948; the unshifted triangle bound 0.991656 is deliberately weak, whereas the shifted bound is $0.02(0.35) + 0.01 = 0.017$. The exact disk maximum is 0.044125, giving a Crouzeix–Palencia bound 0.106527 (over six times the shifted bound). The 2026 proposed constant cannot reverse this comparison.

For a broader comparison, 300 real upper-triangular matrices $F = \left[\begin{smallmatrix} a & b \\ 0 & d \end{smallmatrix}\right]$ were generated with independent $a, d \sim U(-0.75, 0.85)$, $b \sim U(0.1, 1.3)$ and degree-four polynomial coefficients drawn from standard normal variates in the basis centred on $c = (a + d)/2$. These matrices are almost surely non-nilpotent after centring and Schur stable. The elliptical numerical range has semiaxes $\sqrt{(a-d)^2 + b^2}/2$ and $|b|/2$. On its boundary, $\max |p|$ was upper-bounded by a 4096-angle grid plus a Lipschitz margin $\pi A \sum_{j \ge 1} j|c_j| R^{j-1}/4096$, where A is the major semiaxis and $R = |c| + A$. For each shift $\xi \in \{0, c, a, d\}$, write $p(z) = \sum_j d_j (z - \xi)^j$ and compare the exact-power termwise upper bound

$$U_{\text{shift}} = \min_{\xi} \sum_j |d_j| \|(F - \xi I)^j\|_2.$$

Alternative Lyapunov bounds use $\sqrt{\kappa(P)}\alpha^j$ for $j \ge 1$ with P from the scaled discrete Lyapunov equation and 12 fixed contraction-radius candidates per shift. The finite-dimensional Kreiss variant $enw(A)^j$ is dominated by Berger's $2w(A)^j$ and is excluded from the comparison. For the same shifts,

© 2026 by the author(s). Distributed under a Creative Commons CC BY license.

Preprints.org | NOT PEER-REVIEWED | Posted: 23 November 2026 https://doi.org/10.20944/preprints202611.2339.v1

the exact-power termwise estimate also dominates the Berger termwise estimate, so deleting the redundant Kreiss estimate does not change the original ratios. The constant term always uses $\|I\| = 1$.

In the 300-case sample, Crouzeix–Palencia wins against the minimum of the tested baselines in 3 cases (1.0%; Wilson 95% interval approximately 0.34–2.90%), with median ratio 2.054. A non-nilpotent example ($a = -0.43711, d = -0.08075, b = 0.38900$) has exact norm 0.22189, certified grid-plus-margin Crouzeix–Palencia bound 0.56569, shifted bound 0.25291, Lyapunov bound 0.26221. The experimental distribution is illustrative, not representative of all controller polynomials. Polynomial coefficients and individual bounds are archived. This result does not support systematic superiority of the Crouzeix–Palencia method; it identifies the need to select the tightest applicable certificate.

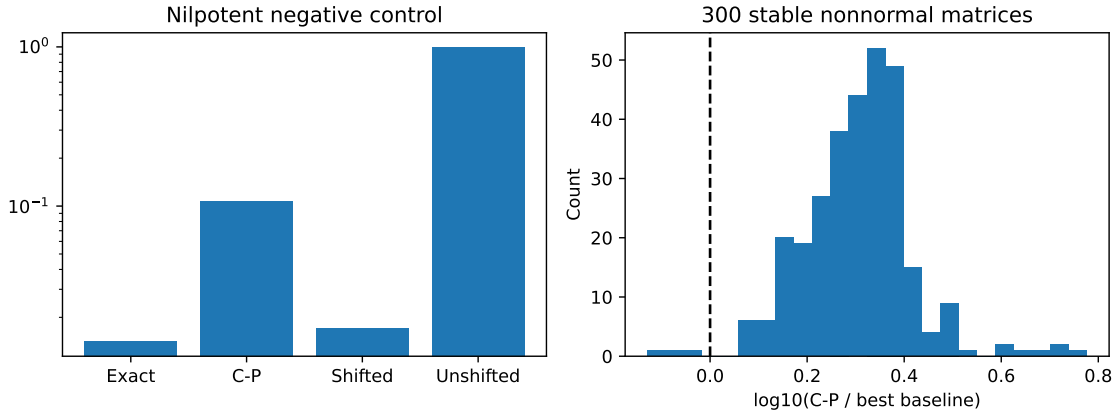


Figure 1. Synthetic negative control and 300 randomly generated stable nonnormal 2×2 matrices. The Crouzeix–Palencia bound is compared with the best of the four-shift termwise and Lyapunov baselines; a positive log ratio indicates a weaker Crouzeix–Palencia bound. Results concern this sampling distribution only.

To test dimensional dependence, a separate 100-case experiment uses 20 matrices from each of five families: random dense nonnormal, Jordan-like triangular, tridiagonal Toeplitz, discretised convection–diffusion and six-state LCL models. Dimensions are 4 and 6, with the LCL family always dimension 6. The polynomial families alternate centred random, alternating coefficients and shifted-filter polynomials of varying degree. For numerical ranges without a closed-form ellipse, 512 support lines define an outer convex polygon. The maximum modulus over the polygon is attained on its boundary. Sampling each edge in eight equal intervals, the maximum sampled modulus plus $\sup_{|z|\le R} |p'(z)|$ times half the largest sampling interval bounds the maximum on the polygon, where R is the largest vertex modulus. A small numerical margin is included in each support value; this is a floating-point enclosure, not interval-arithmetic certification. The comparisons use exact-power shifted termwise bounds, Berger and weighted Lyapunov bounds; shifts include zero, the trace centre and real parts of the eigenvalues. The complete matrices, coefficients and bounds are archived.

The higher-dimensional experiment produces two wins in 100 cases, with median ratio 2.081. The median ratios by family are 1.805 (random), 2.118 (Jordan-like), 2.110 (Toeplitz), 2.358 (convection–diffusion) and 1.937 (LCL). One win occurs in each of the random and LCL families. These small designed ensembles do not estimate performance across all matrices or filters.

© 2026 by the author(s). Distributed under a Creative Commons CC BY license.

Preprints.org | NOT PEER-REVIEWED | Posted: 23 November 2026 https://doi.org/10.20944/preprints202611.2339.v1

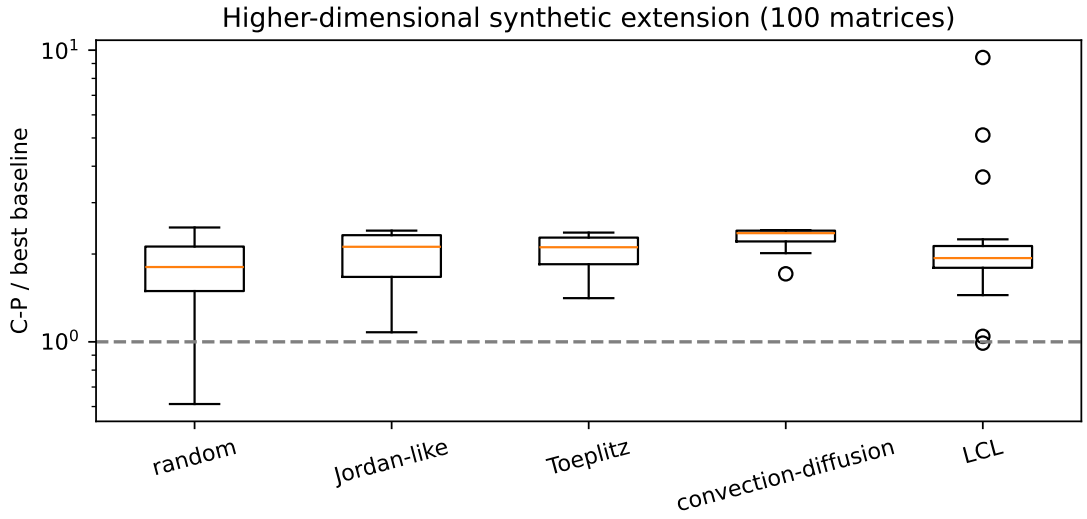


Figure 2. Higher-dimensional extension: ratio of Crouzeix–Palencia to the best tested classical bound, 20 cases in each matrix family. Ratios below one favour Crouzeix–Palencia.

5.6. Implementation and Falsifiable Engineering Questions

Use Ando's exact LMI to synthesise K at declared sample times and documented operating points; verify $w(F_q)$ by an independent angular-support computation; report physical-normalised induced norms, Lyapunov condition numbers, H_∞/Kreiss baselines, achieved polynomial-response norms and measured actuation energy. The scientific question is whether an *optimised non-monomial* output-response criterion yields a non-conservative, hardware-relevant improvement under matched control effort and uncertainty. The 2017 $1+\sqrt{2}$ theorem is sufficient to support the mathematical inequality; no speculative sharp-constant acceptance is required. An advantage is neither assumed nor asserted in the present pilot.

6. Electrical Engineering Translation II: Cycle Covers and Resilient Smart Grids

6.1. What the Graph Theorem Does and Does Not Say

For an undirected finite graph $G = (V, E)$ without bridges, the reported 2026 cycle double cover (CDC) proof claim asserts, subject to specialist refereeing, the existence of a multiset of cycles $\mathcal{C}$ satisfying

$$\sum_{C \in \mathcal{C}} \mathbf{1}[e \in C] = 2, \qquad e \in E. \tag{15}$$

Its proof was recently reported through an AI-generated argument and independently reconstructed in mathematical expositions [6,7]. The claimed conclusion is an *existence* statement on a bridgeless graph. It does not prescribe minimum latency, two edge-disjoint paths between every required source and destination, electromagnetic compatibility, packet reliability or feasible power-flow switching. A radial feeder is a tree, containing bridges; it is not automatically eligible. Engineering work should use a separate meshed *installed* communication graph where each essential link is on a cycle, or design the required augmentation.

6.2. Preconfigured Protection Cycles and the Precise Limitation of CDC

In survivable optical meshes, preconfigured protection cycles (*p-cycles*) provide rapid link recovery. Their design and heuristics predate the 2026 CDC announcement [37–39]. A cycle C can protect an on-cycle link through its alternative arc, and can protect a straddling link whose endpoints lie on the cycle if sufficient spare capacity exists. The CDC incidence requirement $\sum_{C:e\in C} z_C = 2y_e$ does not alone

© 2026 by the author(s). Distributed under a Creative Commons CC BY license.

Preprints.org | NOT PEER-REVIEWED | Posted: 23 November 2026 https://doi.org/10.20944/preprints202611.2339.v1

establish protection capacity, availability, latency or resilience to multiple failures. Given a candidate library of p-cycles, one simplified spare-capacity allocation problem is

$$\begin{aligned} \min_{\{u_C, s_e\}} \quad & \sum_e c_e s_e \\ \text{s.t.} \quad & \sum_C a_{eC} u_C \geq d_e, \quad e \in E_{\text{protected}}, \\ & s_e \geq \sum_{C: e \in C} u_C, \quad u_C \geq 0, \end{aligned} \tag{16}$$

where a_{eC} represents on-cycle or straddling protection capacity in the chosen failure model, u_C is reserved cycle capacity, s_e is installed spare span capacity and d_e is the demand requiring protection. This is a *simplified surrogate*; realistic link-disjoint risk groups, directionality, wavelength continuity and simultaneous failures impose additional constraints. An honest research hypothesis is whether CDC decompositions provide useful warm starts or structure for p-cycle optimisation compared with established survivable-network baselines. The eight-bus feeder pilot is a negative control: its equal restored load with or without CDC rules demonstrates no special CDC benefit.

6.3. Distinguishing Communication Links and Energised Feeders

Let $G^c = (V^c, E^c)$ be the potential communications graph connecting sensors, protection relays, inverters and control centres. Let $y_e \in \{0, 1\}$ indicate whether a communication link is installed and $\ell_e > 0$ its latency. An augmentation decision may minimise cost subject to two-edge-connectivity requirements:

$$\begin{aligned} \underset{y}{\text{minimize}} \quad & \sum_{e \in E^c} c_e y_e, \\ \text{s.t.} \quad & \sum_{e \in \delta(S)} y_e \geq 2, \quad \emptyset \neq S \subsetneq V^c, \end{aligned} \tag{17}$$

assuming all vertices in V^c must be connected. The cut constraints are exponential in number but allow separation by minimum-cut algorithms. The minimum-cost two-edge-connected design problem is NP-hard in general; approximation and survivable-network-design methods provide appropriate baselines [40]. Their presence ensures no selected edge is a bridge, so the installed topology satisfies the hypotheses of the reported CDC claim (subject to specialist refereeing). The companion power graph $G^p = (V^p, E^p)$ must be treated separately, because many electrical distribution networks operate radially even when tie switches physically connect adjacent feeders [41].

If a candidate cycle set $\mathcal{C}_{\text{cand}}$ has been enumerated, an integer cycle-multiplicity variable $z_C \in \{0, 1, 2\}$ may be selected with

$$\sum_{C \in \mathcal{C}_{\text{cand}}: e \in C} z_C = 2 y_e, \qquad e \in E^c. \tag{18}$$

This integer programme does *not* always become feasible with a small pre-enumerated cycle library: if accepted, the reported result guarantees a cover using some collection of cycles, possibly not contained in the restricted candidate set. It is prudent to separate the conditional cover existence from cost-constrained cover discovery. One can use column generation with a cycle pricing subproblem, or treat the cycle cover as a diversity feature and optimise two paths directly.

© 2026 by the author(s). Distributed under a Creative Commons CC BY license.

Preprints.org | NOT PEER-REVIEWED | Posted: 23 November 2026 https://doi.org/10.20944/preprints202611.2339.v1

6.4. Routing, Failure Domains and Latency

For each critical sensor/controller pair (s,t), create binary directed-edge routing variables $x^{(r)}_{e,st}$ for two candidate paths $r \in \{1,2\}$. Flow conservation, link activation and disjointness can be imposed as

$$\sum_{e\in\delta^+(v)} x^{(r)}_{e,st} - \sum_{e\in\delta^-(v)} x^{(r)}_{e,st} = b^{st}_v, \tag{19}$$

$$x^{(r)}_{(u,v),st} + x^{(r)}_{(v,u),st} \le y_{\{u,v\}}, \tag{20}$$

$$x^{(1)}_{(u,v),st} + x^{(1)}_{(v,u),st} + x^{(2)}_{(u,v),st} + x^{(2)}_{(v,u),st} \le 1, \quad \forall\{u,v\} \in E^c. \tag{21}$$

Here $b^{st}_s = 1$, $b^{st}_t = -1$ and $b^{st}_v = 0$ otherwise. The final constraint enforces physical undirected edge-disjointness across both arc orientations. The sum explicitly counts both orientations for both routes, with the undirected edge capacity one; it gives edge-disjoint routes (remove any cycles) but does not address shared poles, utility ducts or control-centre failures. Add shared-risk-link-group inequalities when needed. End-to-end delay requires packet-size, transmission, queueing and processing components, such as

$$\tau^{(r)}_{st} = \sum_e \left(\tau^{\text{tx}}_e + \tau^{\text{prop}}_e + \tau^{\text{queue}}_e\right) x^{(r)}_{e,st} + \tau^{\text{proc}}_{st}. \tag{22}$$

A useful control/communications co-design imposes $\tau^{(r)}_{st} \le \tau^{\max}_{st}$ or a validated probabilistic delay tail; constant per-edge delay is only a first-order surrogate.

Under *independent* individual-link failure events, a path with edge survival probabilities $1-p_e$ has reliability $R_r = \prod_{e\in P_r}(1-p_e)$. For truly edge-disjoint paths whose failure mechanisms are independent,

$$R_{\text{parallel}} = 1 - (1-R_1)(1-R_2). \tag{23}$$

Correlated weather, power supply or cyber failures invalidate this independence formula. A strong engineering contribution must therefore optimise both structural redundancy and empirically supported dependency models.

6.5. Feasible Distribution Restoration: Radiality and Electrical Physics

For a distribution grid, let $u_i \in \{0,1\}$ denote whether bus i is supplied, and $x^p_{ij} \in \{0,1\}$ whether a line is energised. For a single-source fully served tree,

$$\sum_{(i,j)\in E^p} x^p_{ij} = |V^p| - 1 \tag{24}$$

alone is insufficient for connectivity: enforce root-to-bus commodity flows with available capacities and flow balance, or a validated spanning-tree formulation. For partially restored islands, the edge-count relation must be modified for the number of energised vertices and islands. Using a radial orientation and the branch-flow (DistFlow) model,

$$\begin{aligned} P_{ij} &= p_j + \sum_{k:j\to k} P_{jk} + r_{ij}\ell_{ij}, \\ Q_{ij} &= q_j + \sum_{k:j\to k} Q_{jk} + x_{ij}\ell_{ij}, \\ v_j &= v_i - 2(r_{ij}P_{ij} + x_{ij}Q_{ij}) + (r^2_{ij} + x^2_{ij})\ell_{ij}, \\ v_i\ell_{ij} &= P^2_{ij} + Q^2_{ij}, \end{aligned} \tag{25}$$

where $v_i = |V_i|^2$ and $\ell_{ij} = |I_{ij}|^2$. The equality in the final line is nonconvex; replacing it by $v_i\ell_{ij} \ge P^2_{ij} + Q^2_{ij}$ gives the branch-flow second-order-cone relaxation analysed by Farivar and Low; its exactness

© 2026 by the author(s). Distributed under a Creative Commons CC BY license.

Preprints.org | NOT PEER-REVIEWED | Posted: 23 November 2026 https://doi.org/10.20944/preprints202611.2339.v1

requires stated assumptions and is not guaranteed in every switched restoration instance [42]. Integrate switch statuses with big-M constraints or indicator constraints, voltage bounds, inverter reactive-power support, thermal limits and protection coordination.

A combined *proposed* objective is

$$\begin{aligned} \min\ J = {} & w_U \sum_i P_i^{\mathrm{load}}(1-u_i) \\ & + w_L \sum_{(i,j)\in E^p} r_{ij}\ell_{ij} \\ & + w_S \sum_{e\in E^p} |x_e^p - x_{e,0}^p| \\ & + w_C \sum_{e\in E^c} c_e y_e + w_D \sum_{(s,t),r} \tau_{st}^{(r)}. \end{aligned} \tag{26}$$

subject to (17)–(25). The weights must be normalised to comparable units or interpreted as economic costs; unconstrained arbitrary weights would undermine conclusions. In practice, network design (y), controller-path selection, and electrical restoration (x^p, u) may operate on different time scales, so decomposition into design and operational stages is usually more credible than a single monolithic solve.

6.6. A Transparent Reliability Illustration

Suppose two edge-disjoint paths each contain two links with independent availability 0.99. Then each path has $R_1 = R_2 = (0.99)^2 = 0.9801$, and the idealised parallel success rate is $1 - (0.0199)^2 = 0.99960399$. The numerical difference illustrates the value of independent redundancy, *not* an improvement guaranteed by the reported cycle double cover claim, and not an observed smart-grid reliability measurement. To make this publishable, model correlated failures, physical shared-risk groups, packet latencies, link costs, N-1 and N-2 contingencies, and reconfiguration time on IEEE 33- and 69-node distribution feeders with a separately meshed communications layer.

6.7. Research Hypotheses and Evaluation Protocol

Research question G1: do CDC-generated p-cycle candidates offer measurable spare-capacity, setup-time, or routing advantages over established p-cycle and two-edge-connected baseline designs under the same cost and shared-risk model? Research question G2: can cyber–physical integration recover more load or reduce operational delay than power-only restoration under externally specified communication failures? Neither proposed benefit has yet been demonstrated in the synthetic test. Baselines must include disjoint-path integer optimisation *without* CDC features, minimum-cut topology augmentation, classic reconfiguration and a no-communication-delay oracle. Metrics include cost, cycle-cover feasibility, protected bus fraction, load not served, ENS/MWh, outage minutes, recovery time, voltage deviations, packet delivery ratio and 95th/99th percentile latency. A further novelty test should quantify whether CDC features improve the solution beyond the simpler edge-connectivity properties already provided by Menger's theorem [43].

7. Electrical Engineering Translation III: Lattice Complexity and Adaptive MIMO Reception

7.1. AI-Assisted CVP Complexity as a Design Constraint

The closest vector problem (CVP) asks, given a basis $B \in \mathbb{R}^{m\times n}$ and target $y \in \mathbb{R}^m$, to find $z \in \mathbb{Z}^n$ minimising $\|y - Bz\|$. Approximation complexity is a distinct question: for which factors $\gamma(n)$ is it computationally hard to guarantee $\|y - B\hat{z}\| \le \gamma(n)\ \min_z \|y - Bz\|$ on *all* input lattices? A 2026 technical report claims deterministic NP-hardness of Euclidean GapCVP$_2$ approximation by a factor $n^{1/400}$ for rank n, under deterministic polynomial-time reductions [21]. This is a worst-case result, not a BER prediction. Aharonov and Regev established $\sqrt{n}$-factor CVP approximation in NP $\cap$ coNP,

© 2026 by the author(s). Distributed under a Creative Commons CC BY license.

Preprints.org | NOT PEER-REVIEWED | Posted: 23 November 2026 https://doi.org/10.20944/preprints202611.2339.v1

constraining the plausible hardness boundary [44]. Sphere-decoding hardness and complexity issues long predate AI: exact lattice decoding was already recognised as computationally hard and Jaldén–Ottersten established exponential expected sphere-decoding complexity at fixed SNR [45]. It is *not* an algorithm for lattice decoding, nor does it imply that a realistic random fading channel is necessarily as hard as an adversarial lattice. This distinction turns a negative theorem into an engineering research strategy: exploit the *structure of the wireless channel and the finite constellation*, choose a receiver matched to the instance, and document the conditions under which low complexity is obtained.

7.2. Whitened Finite-Constellation Maximum-Likelihood Problem

For an $N_r \times N_t$ narrowband channel at one orthogonal-frequency-division-multiplexing resource element,

$$\begin{aligned} y &= Hs + n, \qquad s \in \mathcal{S}^{N_t}, \\ n &\sim \mathcal{CN}(\mathbf{0}, R_n). \end{aligned} \tag{27}$$

Here $\mathcal{CN}(\mathbf{0}, R_n)$ denotes the circularly symmetric complex Gaussian distribution with zero mean and noise covariance R_n. When R_n is known positive definite, whiten using $y' = R_n^{-1/2} y$ and $G = R_n^{-1/2} H$. The maximum-likelihood detector is

$$\boxed{\widehat{s}_{\mathrm{ML}} = \arg\min_{s \in \mathcal{S}^{N_t}} \left\| y' - Gs \right\|_2^2.} \tag{28}$$

For M-ary QAM this enumerates up to M^{N_t} candidates. Conversion to a real-valued problem uses

$$\widetilde{y} = \begin{bmatrix} \Re y' \\ \Im y' \end{bmatrix}, \quad \widetilde{G} = \begin{bmatrix} \Re G & -\Im G \\ \Im G & \Re G \end{bmatrix}, \quad \widetilde{s} = \begin{bmatrix} \Re s \\ \Im s \end{bmatrix}, \tag{29}$$

with the finite QAM alphabet restrictions maintained. If $N_r \geq N_t$ and $\widetilde{G}$ is full column rank, let $\widetilde{G} = QR$ be a thin QR decomposition, and set $z = Q^T \widetilde{y}$. The cost separates into a constant orthogonal residual and an upper-triangular search:

$$\left\| \widetilde{y} - \widetilde{G}\widetilde{s} \right\|^2 = \| z - R\widetilde{s} \|^2 + \left\| (I - QQ^T)\widetilde{y} \right\|^2. \tag{30}$$

For $R = [r_{ij}]_{i,j=1}^{n}$, the exact finite-alphabet search cost is

$$D(\widetilde{s}) = \sum_{i=1}^{n} \left| z_i - \sum_{j=i}^{n} r_{ij} s_j \right|^2, \quad n = 2N_t. \tag{31}$$

Every term is nonnegative, so a partial suffix metric at search level i is a *valid lower bound* on the cost of any completion. This is the mathematical basis of sphere decoding and exact pruning, whose complexity may nevertheless be large in unfavourable channel/SNR regimes [46,47].

7.3. Complexity-Aware Hybrid Detection Architecture

We propose an adaptive receiver that uses a cheap channel-conditioned baseline, a bounded-width candidate search and an optional exact certificate. Define the effective noise scale σ^2, condition number $\kappa(G)$ and an initial Babai/MMSE estimate s_{B}. Set a feasible radius $D_0 = \| y' - Gs_{\mathrm{B}} \|^2$ after slicing the Babai/MMSE point s_{B} onto the admissible finite constellation. Candidate ranking can be based on

$$\eta = \alpha_1 \log \kappa(G) + \alpha_2 \log(1 + \sigma^2) + \alpha_3 N_t + \alpha_4 \log M, \tag{32}$$

where α_j are trained on a separate data partition. This score is an empirical *controller of complexity*, not a theorem about exact decoding. List/K-best and fixed-complexity sphere decoders are established techniques; a scientifically new claim would require an improved valid certificate, a proven

© 2026 by the author(s). Distributed under a Creative Commons CC BY license.

Preprints.org | NOT PEER-REVIEWED | Posted: 23 November 2026 https://doi.org/10.20944/preprints202611.2339.v1

performance-complexity regime, or hardware measurements beyond these baselines [45,47]. It selects a candidate width $K_{\text{list}}(\eta)$ and maximum search budget $B_{\max}$. At each layer, retain at most K_{list} best suffixes by partial cost, and return the best complete finite-alphabet candidate. A learned ranking model may reorder candidates, but it may not remove a candidate from an *exact* branch-and-bound search without a valid lower-bound certificate.

A mathematically safe *exactness test* is available if the algorithm also computes a lower bound $L_{\text{unexplored}}$ on every unvisited branch. If the best complete candidate has cost U, then

$$U \le L_{\text{unexplored}} \quad \Longrightarrow \quad s_{\text{returned}} = s_{\text{ML}}, \tag{33}$$

up to ties. At a truncated candidate-list stage, a branch excluded solely because of a K-best width generally has *unknown* optimum, so (33) must not be asserted. One option is to run a budget-limited exact search after list detection and report three classes of output: certified ML, uncertified approximate, and timeout. Another is to use a proven relaxation lower bound $L_{\text{relax}} \le D_{\text{ML}}$. With $U = D(s_{\text{returned}})$, the additive gap $U - L_{\text{relax}}$ provides a reproducible instance-specific suboptimality certificate even when exactness is not achieved.

7.4. A Receiver Optimisation Objective

For a given latency budget $T_{\max}$ and implementation hardware h, a proposed training/architecture objective is

$$\begin{aligned} \min_{\pi} \quad & \mathbb{E}[\text{BLER}(\pi; H, n)] + \beta \mathbb{E}[\text{Energy}(\pi)] \\ & + \gamma \Pr\{T(\pi) > T_{\max}\}, \end{aligned} \tag{34}$$

where π maps observed features to an algorithm and per-instance budget. Expectations must be over an explicitly defined channel ensemble; results for correlated Rayleigh fading may not transfer to measured mmWave channels or high-mobility industrial environments. Hardness results preclude an unsupported claim of universal fast worst-case CVP approximation; they do not preclude instance-adaptive speed-ups under a stated wireless distribution. Baselines should include MMSE, zero forcing, fixed K-best, Schnorr–Euchner sphere decoding, list sphere decoding and an exhaustive ML oracle for small antenna configurations.

7.5. Concrete Experiments and Implementable Radio System

An initial setup could use $N_t \in \{2, 4, 8\}$, $N_r \ge N_t$, 16-QAM and 64-QAM, SNR from 0 to 30 dB, uncorrelated and spatially correlated channels, imperfect CSI, finite-resolution ADC and unequal received powers. A reproducible open implementation should archive all pseudo-random seeds, channel coefficients and detected vectors, then report BER, BLER, average/95th/99th-percentile latency, MAC operations, peak memory, fraction of certified-ML detections, and confidence intervals. An FPGA prototype should report bit width, clock period, throughput, DSP slice utilisation and measured energy per decoded information bit. The hypothesis is not merely that AI can decode MIMO, but that mathematical complexity awareness plus exactness/gap certificates provides a more transparent latency–performance trade-off than either a fixed detector or an opaque learned model.

7.6. Illustrative MIMO Study (Executed Python Reference)

For each of 10, 14 and 18 dB, 10,000 independent 2×2 complex Rayleigh channel frames with 16-QAM and two streams were simulated. The SNR convention is per transmitted complex symbol E_s/N_0, where $E_s = 1$, $H_{ij} \sim \mathcal{CN}(0,1)$, $n_i \sim \mathcal{CN}(0, 10^{-\text{SNR}/10})$ and there is no $1/\sqrt{2}$ stream-power scaling. Perfect CSI is assumed. The exhaustive ML oracle evaluates 256 complete candidate vectors. The real QR K-best implementation evaluates partial metrics at each of four real tree levels, with widths 2 and 8. The certificate is issued only when the returned candidate metric is below every discarded partial lower bound (a 10^{-10} numerical margin is required); the oracle is used only for validation.

© 2026 by the author(s). Distributed under a Creative Commons CC BY license.

Preprints.org | NOT PEER-REVIEWED | Posted: 23 November 2026 https://doi.org/10.20944/preprints202611.2339.v1

Table 5 reports symbol error rates (SER) with approximate 95% confidence intervals based on independent frames, treating the two errors within a frame as a cluster. Certification proportions use Wilson intervals. Visited candidates count metric evaluations (partial for K-best, complete for ML), not cycle-accurate MACs or wall-clock latency. K=2 visits 28 tree nodes and K=8 visits 84; QR, sorting and MMSE costs are excluded, so node counts are not a hardware speed-up claim. At 10 dB the paired K=8 minus ML SER difference is 0.00080 (95% CI $[-0.00007, 0.00167]$); at 18 dB it is 0.00060 (95% CI $[0.00003, 0.00117]$). Every reported certificate agreed with the exhaustive oracle. Larger dimensions, imperfect CSI, coding, correlated channels and hardware latency remain untested.

Table 5. Synthetic 2-by-2 16-QAM reference, 10,000 independent transmissions per SNR. Parentheses contain 95% intervals. Node counts are partial/complete metric evaluations and do not include preprocessing; no hardware validation.

SNR (dB)	Detector	SER (95% CI)	Certified ML (95% CI)	Metric evaluations
10	ML	0.2736 (0.2661–0.2811)	–	256
10	MMSE	0.3482 (0.3408–0.3555)	–	–
10	K2	0.2912 (0.2836–0.2988)	0.8132 (0.8054–0.8207)	28
10	K8	0.2744 (0.2669–0.2819)	0.9848 (0.9822–0.9870)	84
14	ML	0.1064 (0.1010–0.1117)	–	256
14	MMSE	0.1938 (0.1876–0.2001)	–	–
14	K2	0.1201 (0.1144–0.1258)	0.8943 (0.8881–0.9002)	28
14	K8	0.1069 (0.1015–0.1123)	0.9921 (0.9902–0.9937)	84
18	ML	0.0261 (0.0232–0.0289)	–	256
18	MMSE	0.0895 (0.0848–0.0942)	–	–
18	K2	0.0362 (0.0329–0.0396)	0.9560 (0.9518–0.9598)	28
18	K8	0.0267 (0.0238–0.0295)	0.9963 (0.9949–0.9973)	84

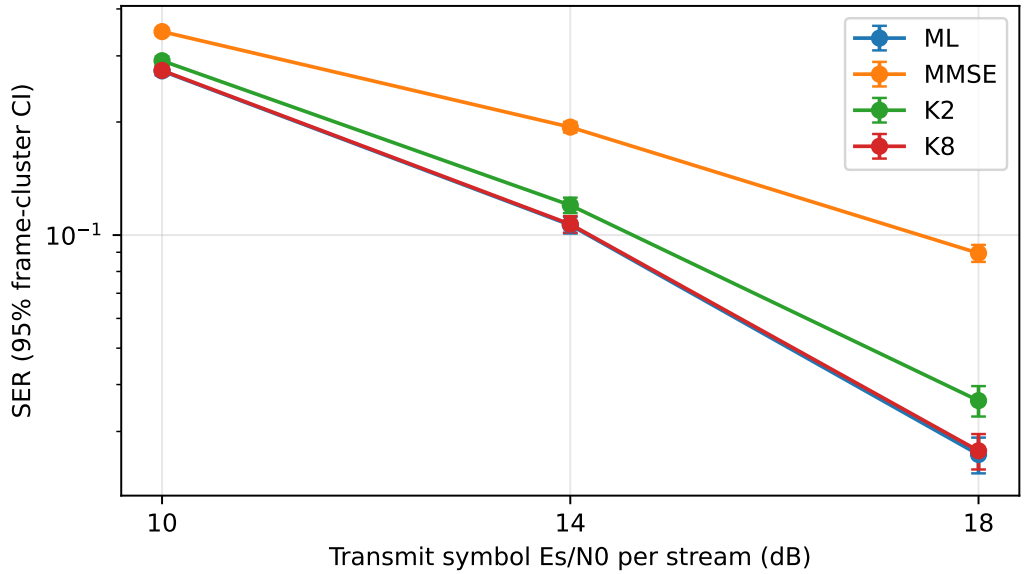


Figure 3. Synthetic 2-by-2 16-QAM SER; 10,000 independent frames per SNR with frame-cluster 95% confidence intervals. No FPGA or real-time implementation.

8. Electrical Engineering Translation IV: Global Identifiability in Digital Twins and Sensor Networks

8.1. Why a Jacobian Counterexample Matters for Engineering

The complex polynomial Jacobian conjecture asks whether a polynomial map $h : \mathbb{C}^n \to \mathbb{C}^n$ with constant nonzero Jacobian determinant must have a polynomial inverse. A 2026 preprint claims complex-polynomial higher-dimensional counterexamples challenging this global conclusion for

© 2026 by the author(s). Distributed under a Creative Commons CC BY license.

Preprints.org | NOT PEER-REVIEWED | Posted: 23 November 2026 https://doi.org/10.20944/preprints202611.2339.v1

$n \geq 3$ under the stated complex-polynomial setting; the two-dimensional question is not thereby settled [19]. A much simpler real counterexample already makes the engineering point: $h(x,y) = (e^x \cos y, e^x \sin y)$ has determinant $e^{2x} > 0$ but is not injective on any y-domain spanning more than 2π. Real polynomial Pinchuk counterexamples have been known since 1994, and multiple AC power-flow solutions are classical [48,49]. Therefore a debated 2026 complex-polynomial counterexample is *not* necessary to motivate sensor identifiability. This warning applies to nonlinear sensor fusion, battery state-of-charge/health identification, converter parameter estimation and digital twins with multiple admissible operating points. It does *not* imply that practical measurement maps necessarily inherit the same algebraic counterexample.

8.2. Measurement and Dynamic-State Formulation

Let the physical state $x \in D \subset \mathbb{R}^n$ include selected bus voltages/angles, power-electronic parameters, thermal states, or battery variables. Measurements are

$$y = h(x) + \varepsilon, \qquad \|\varepsilon\|_2 \leq \delta, \tag{35}$$

where $h : D \to \mathbb{R}^m$ is continuously differentiable. A weighted least-squares digital-twin estimate often solves

$$\widehat{x} = \arg\min_{x \in D} \big(h(x) - y\big)^T R^{-1} \big(h(x) - y\big), \tag{36}$$

subject to thermal, power balance and state-of-charge constraints. The common test $\operatorname{rank}(J_h(x)) = n$ for each x is necessary for regular local inversion in an n-dimensional state; it does not automatically rule out two distant states $x_1 \neq x_2$ giving $h(x_1) = h(x_2)$. In rectangular systems $m > n$, even uniform positivity of $J_h^T J_h$ only provides a strong *local* sensitivity bound, not a global injectivity guarantee without further conditions.

8.3. Classical Strong-Monotonicity Criterion and Its Engineering Meaning

Global injectivity via strong monotonicity is a *classical theorem*, not a contribution originating in this manuscript [49,50]. A checkable sufficient condition can be imposed on an *appropriate square measurement projection*. Suppose D is convex, $L \in \mathbb{R}^{n \times m}$ is fixed, $g(x) = Lh(x)$ and

$$\boxed{\frac{J_g(x) + J_g(x)^T}{2} \succeq m_0 I_n, \quad \forall x \in D, \quad m_0 > 0.} \tag{37}$$

The following proposition restates the standard implication and an elementary noise-error consequence for engineering clarity.

Proposition 1. *If g is continuously differentiable on a convex domain D and (37) holds, then g is injective on D and*

$$\|g(x) - g(z)\|_2 \geq m_0 \|x - z\|_2, \quad \forall x, z \in D. \tag{38}$$

For two candidate states $x^\star, \widehat{x} \in D$, with measurement equation $Ly = g(x^\star) + e$, where $\|e\| \leq \delta_g$, if $\|g(\widehat{x}) - Ly\| \leq \delta_g$ then

$$\boxed{\|\widehat{x} - x^\star\|_2 \leq 2\delta_g / m_0.} \tag{39}$$

Proof. Let $d = x - z$. Convexity of D ensures the whole segment $z + td$ is in D, and the fundamental theorem of calculus gives

$$g(x) - g(z) = \int_0^1 J_g(z + t(x - z))(x - z)\, \mathrm{d}t. \tag{40}$$

© 2026 by the author(s). Distributed under a Creative Commons CC BY license.

Preprints.org | NOT PEER-REVIEWED | Posted: 23 November 2026 https://doi.org/10.20944/preprints202611.2339.v1

Multiplying by d^T and using (37) yields

$$d^T(g(x) - g(z)) \geq m_0\|d\|_2^2. \tag{41}$$

Cauchy–Schwarz gives $\|g(x) - g(z)\|\|d\| \geq m_0\|d\|^2$, proving (38), including injectivity. Finally, triangle inequality gives $\|g(\hat{x}) - g(x^\star)\| \leq \|g(\hat{x}) - Ly\| + \|e\| \leq 2\delta_g$, which proves (39). □

If $\|\varepsilon\| \leq \delta$ in the unprojected measurements, one may use $\delta_g \leq \|L\|_2\delta$. This sufficient condition may be *strong*, especially for nonlinear AC power-flow maps, but it provides a genuine global alternative to a local Jacobian-rank test. Replacing the uniform condition by samples at grid points without a bound between them would *not* be rigorous.

8.4. Constructing and Verifying a Useful Projection

The engineering design variables can include the measurement subset, sensor calibration and linear projection L. For instance, a proposed robust formulation is

$$\min_{L,m_0} \quad \mu\|L\|_F^2 - m_0 \tag{42}$$

$$\text{s.t.} \quad \frac{LJ_h(x) + J_h(x)^T L^T}{2} \succeq m_0 I, \quad \forall x \in D,$$

$$\|L\|_F \leq L_{\max}, \quad m_0 \geq \epsilon. \tag{43}$$

For $\mu \geq 0$, the objective is convex and all pointwise matrix inequalities are affine in (L, m_0). This is equivalent to maximising the concave original objective. The infinitely many x-constraints make it a robust convex programme, not automatically a finite SDP. If an *interval enclosure* $J_h(x) \in \{J_0 + \sum_q \alpha_q J_q : |\alpha_q| \leq 1\}$ is *valid for all* $x \in D$, conservative sufficient constraints at all vertices or a norm-bounded robust LMI can certify the required condition. A finite sample grid without an enclosure only suggests likely identifiability.

As a simple illustration, take $h(x) = Ax + \phi(x)$ with $A = A^T \succeq 2I$, and assume $\|J_\phi(x)\|_2 \leq 0.3$ everywhere on a convex admissible domain. Then

$$\frac{J_h + J_h^T}{2} \succeq (2 - 0.3)I = 1.7I, \tag{44}$$

and (39) becomes $\|\hat{x} - x^\star\| \leq (2/1.7)\delta$ for $L = I$ and residual tolerance δ. This analytical calculation is valid without asserting that a particular battery or AC-network measurement model satisfies the premises. The next step is to derive enclosures for the *actual* chosen model and to quantify the region of state space over which uniqueness is guaranteed.

8.5. Power-System and Battery Digital-Twin Use Cases

For an AC network, a standard injection measurement at bus i is

$$P_i = V_i \sum_j V_j(G_{ij}\cos\theta_{ij} + B_{ij}\sin\theta_{ij}), \tag{45}$$

$$Q_i = V_i \sum_j V_j(G_{ij}\sin\theta_{ij} - B_{ij}\cos\theta_{ij}). \tag{46}$$

Voltage magnitudes, phasors, branch flows and smart-meter readings form $h(x)$. The state may include voltage angles and magnitudes, minus a reference angle. For a battery state estimator, a typical measurement may combine

$$\begin{aligned} v_t &= \mathrm{OCV}(\mathrm{SoC}) - Ri - v_{\mathrm{RC}}, \\ \dot{\mathrm{SoC}} &= -\frac{i}{Q_{\mathrm{nom}}}. \end{aligned} \tag{47}$$

© 2026 by the author(s). Distributed under a Creative Commons CC BY license.

Preprints.org | NOT PEER-REVIEWED | Posted: 23 November 2026 https://doi.org/10.20944/preprints202611.2339.v1

with temperature and current readings. If capacity is specified in ampere-hours, $\dot{\mathrm{SoC}} = -i/(3600 Q_{\mathrm{nom,Ah}})$ for t measured in seconds. An OCV curve with flat regions may make state reconstruction badly conditioned, even when a local numerical solver converges. The proposed method would identify a certified operating subset or add measurements until a global error bound becomes possible. Baselines include standard weighted least squares, extended and unscented Kalman filters, multiple-start nonlinear least squares and interval observers [51]. Evaluation should report ambiguous solutions, worst-case sensor noise amplification, real-time inference cost, confidence calibration and the fraction of the physical operating range covered by a valid certificate.

8.6. Battery-Inspired Overdetermined Measurement and Global-Error Pilot

Set $x = (s, v_{\mathrm{RC}})$, $s \in [0,1]$, $v_{\mathrm{RC}} \in [-0.15, 0.15]$, with three synthetic measurements (two auxiliary channels are hypothetical):

$$\begin{aligned} h_1(x) &= 3.6 + 0.07s + 0.015 \tanh[12(s-0.5)] - v_{\mathrm{RC}}, \\ h_2(x) &= 0.5s + 0.2 v_{\mathrm{RC}}, \\ h_3(x) &= 0.15s - 0.25 v_{\mathrm{RC}}. \end{aligned} \tag{48}$$

Let $J_0 = \begin{bmatrix} 0.07 & -1 \\ 0.5 & 0.2 \\ 0.15 & -0.25 \end{bmatrix}$, $L = J_0^{\dagger}$ and $g = Lh$. The third measurement has distinct sensitivities rather than repeating the second. The Jacobian perturbation is $\beta e_1 e_1^T$ with $0 \le \beta \le 0.18$ (rectangular first factor understood), so the minimum eigenvalue is bounded at the two endpoints:

$$\frac{J_g + J_g^T}{2} = I + \beta\, \mathrm{sym}((Le_1)e_1^T) \succeq m_0 I, \quad m_0 = 0.93647. \tag{49}$$

For independent Gaussian noise with covariance $\Sigma = \mathrm{diag}(0.002^2, 0.003^2, 0.003^2)$, set $\Sigma_g = L\Sigma L^T$ and $\delta_{0.95} = \sqrt{\lambda_{\max}(\Sigma_g)\chi^2_{2,0.95}} = 0.013900$. Indeed $\Sigma_g^{-1/2} L\varepsilon$ is standard bivariate Gaussian, so $\|L\varepsilon\| \le \delta_{0.95}$ with probability at least 0.95. The deployable bound uses only the data, estimator and known noise model:

$$\|\widehat{x} - x^{\star}\|_2 \le \frac{\|L(h(\widehat{x}) - y)\|_2 + \delta_{0.95}}{0.93647},$$

with probability at least 0.95 (conditional on the nominal model and calibrated noise covariance), not a deterministic per-sample guarantee. No realised noise is used by the estimator. Two thousand weighted least-squares trials with uniformly sampled interior states produced median error 0.00436, 95th percentile 0.01103, mean unprojected residual 0.002335, and empirical coverage 99.50% (Wilson 95% CI 99.08–99.73%). The conservatism is expected from the spectral covariance envelope.

As a negative control, change the nominal sensor law to $h_1 = 3.6 + 0.0001s - v_{\mathrm{RC}}$, $h_2 = -0.001s + 0.2 v_{\mathrm{RC}}$ and $h_3 = -0.0003s - 0.25 v_{\mathrm{RC}}$, representing a flat OCV region with weak reversed auxiliary sensitivities. Its Jacobian still has rank 2 and smallest singular value 0.001027, but for the same calibrated projection L, $\lambda_{\min}(\mathrm{sym}(LJ_h)) = -0.001945$. The nominal certificate fails; it must not be applied. Over 2000 independent trials the median and 95th-percentile errors were 0.45924 and 0.90117. This tests the distinction between local rank and a robust global certificate for a specified projection, not noninjectivity of this affine example; a new projection may re-establish monotonicity but amplify noise. No real cell is represented.

© 2026 by the author(s). Distributed under a Creative Commons CC BY license.

Preprints.org | NOT PEER-REVIEWED | Posted: 23 November 2026 https://doi.org/10.20944/preprints202611.2339.v1

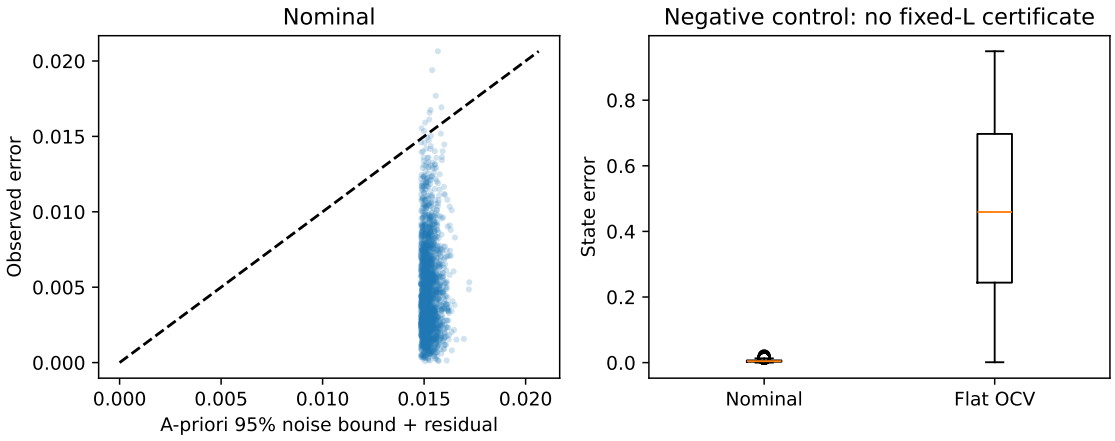


Figure 4. Synthetic overdetermined battery-inspired observations, 2000 nominal and 2000 flat-OCV trials. Left: a-priori 95% noise envelope plus measured residual, conditional on known covariance; right: error distributions for a full-rank but fixed-projection certificate failure. Not a physical battery experiment.

9. Additional Mathematical Routes to New Electrical-Electronic Technology

9.1. Hadamard Matrices for Multiplexed Sensors and Channel Training

A Hadamard matrix $H \in \{\pm 1\}^{n\times n}$ satisfies $H^T H = nI$. Twelve newly constructed Hadamard orders (668, 716, 892, 1132, 1244, 1388, 1436, 1676, 1772, 1916, 1948 and 1964) were independently analysed in 2026, while the general Hadamard conjecture remains open [27]. The construction is a K-type result; any performance improvement over existing Sylvester/Walsh matrices with padding must be demonstrated under equal energy and resource budgets. The direct engineering relevance comes from orthogonality, not from the mere fact that a new order was discovered. Suppose a linear sensing or radio calibration model has n unknown coefficients arranged in a, with n training measurements $y = Xa + \varepsilon$ and $\varepsilon \sim \mathcal{N}(0, \sigma^2 I)$. Select

$$X = \sqrt{E/n}\, H \quad \Longrightarrow \quad X^T X = EI. \tag{50}$$

The least-squares estimator $\widehat{a} = (X^T X)^{-1} X^T y$ then has covariance

$$\boxed{\mathrm{Cov}(\widehat{a} - a) = \frac{\sigma^2}{E} I.} \tag{51}$$

At equal column energy, orthogonal designs minimise noise coupling and offer simple inverses. The actual design can use bipolar switching patterns to interrogate a sensor array, orthogonal pilot signals in a linear MIMO estimation model, or coded measurements in an analogue front-end. Necessary application conditions include sign-switch feasibility, ADC dynamic range, synchronisation, phase drift, nonnegative intensity constraints for optical systems, and the number of independently addressable physical channels. New matrix orders make additional design lengths possible; they do not imply an automatic advantage over existing Walsh orders after padding and truncation. An experimental study should compare estimation MSE, peak-to-average power, implementation switching energy and sensitivity to missing measurements.

9.2. A Polynomial-Geometry Research Hypothesis for Digital Filtering

For a stable causal IIR filter $H(z) = B(z)/A(z)$, poles of A govern stability while poles and zeros jointly determine frequency response and coefficient sensitivity. Sendov's conjecture, now reported proved, concerns the proximity of a root of a polynomial with all roots in the unit disk to a root of its

© 2026 by the author(s). Distributed under a Creative Commons CC BY license.

Preprints.org | NOT PEER-REVIEWED | Posted: 23 November 2026 https://doi.org/10.20944/preprints202611.2339.v1

derivative [20]. For a polynomial $A(z) = \prod_{j=1}^{n}(z - \lambda_j)$, logarithmic differentiation away from roots gives

$$\frac{A'(z)}{A(z)} = \sum_{j=1}^{n} \frac{1}{z - \lambda_j}. \tag{52}$$

Critical-point geometry thus describes cancellation of forces generated by zeros. However, actual pole sensitivity to an additive coefficient perturbation obeys, at a simple pole λ,

$$\Delta\lambda \approx -\frac{\Delta A(\lambda)}{A'(\lambda)}. \tag{53}$$

Sendov's distance bound *alone* neither lower bounds $|A'(\lambda)|$ nor bounds (53). Therefore a research programme must derive an *additional* relationship between root/critical-point distributions, fixed-point coefficient quantisation and filter performance, rather than claiming the solved theorem already stabilises filters. Test 8-, 12- and 16-bit implementations, pole-margin distributions and worst-case passband error against established pole-placement and lattice-filter baselines.

9.3. Fast Matrix Multiplication: When Asymptotic Improvements Matter

A 2026 preprint reports $\omega_{\mathbb{C}} \leq 9/4$ for exact scalar arithmetic over the complex numbers, with constructive follow-up arguments and results over other fields [29]. This is an arithmetic-operation exponent, not a floating-point runtime theorem. The exponent is defined by the existence of algorithms performing dense $n \times n$ multiplication in $O(n^{\omega+\epsilon})$ arithmetic operations for any fixed $\epsilon > 0$ under the respective formal assumptions. If an electrical digital twin performs repeated large dense products (for example, block state propagation or batched sensitivity Jacobians), a theoretical acceleration is conceivable. Yet for realistically sized systems, the hidden constants, recursion depth, data movement, finite-word-length stability, hardware topology and sparsity pattern dominate. An implementable study should distinguish a theoretical *asymptotic arithmetic count* from measured execution time, compare with vendor-optimised BLAS and sparse linear algebra, and verify that error propagation remains acceptable for power-system state estimation or MIMO covariance operations. The discovered exponent is not itself a new FPGA multiplication circuit.

9.4. Graph Extremal Theory and Sparse Routing Algorithms

AI-supported resolutions of particular Erdős–Sós, Turán, Ramsey and graph-degeneracy questions [21,23,24] provide extremal limits for embeddings or configurations. They can supply adversarial graph families for stress-testing communication backbones, but a theorem about generic graphs does not automatically preserve capacities, geographic constraints or electrical radiality. Separately, the 2026 subquadratic 3SUM and subcubic all-pairs shortest-path results are algorithmic complexity results in specified computational models [32]; they may inspire route-computation kernels only when weights, graph density, required precision and practical graph sizes match those models. Publishable improvements should compare worst-case and measured average-case scaling against Dijkstra, Bellman–Ford, Johnson and relevant sparse graph methods, not just quote asymptotic exponents.

9.5. Formal Discovery and Optimal Saddle-Point Control

The 2026 anchored-gradient work reports a particular last-iterate statement [25], but extra-anchored-gradient methods already obtained $O(1/k^2)$ rates for the *squared gradient norm* of smooth convex–concave games in 2021 [52]. Any engineering comparison must specify the rate metric, assumptions and algorithm, and include EAG/FEG and direct KKT solvers for quadratic–bilinear cases. Robust control and minimax dispatch can be written abstractly as

$$\min_{u \in \mathcal{U}} \max_{w \in \mathcal{W}} L(u, w) = \tfrac{1}{2} u^T Q u + u^T G w - \tfrac{1}{2} w^T R w + c^T u + d^T w, \tag{54}$$

© 2026 by the author(s). Distributed under a Creative Commons CC BY license.

Preprints.org | NOT PEER-REVIEWED | Posted: 23 November 2026 https://doi.org/10.20944/preprints202611.2339.v1

with $Q \succeq 0$, $R \succeq 0$ and convex feasible sets. The saddle operator is

$$T(u,w) = \begin{bmatrix} \nabla_u L(u,w) \\ -\nabla_w L(u,w) \end{bmatrix}. \tag{55}$$

If the hypotheses of the published convergence theorem apply (including the correct anchoring scheme, regularity and step-size restrictions), one can transfer its convergence guarantee to a convex–concave *surrogate* of robust resource allocation. Realistic inverter design with switching, nonlinear AC power flow, discrete protection and nonconvex chance constraints generally does *not* meet these assumptions without relaxation. The research task is to construct a truthful convex surrogate, prove its relationship to the physical system, and measure last-iterate feasibility and convergence against standard projected gradient, extragradient, ADMM and model-predictive controllers.

9.6. Packing, Coding and Wireless Feasibility

Let $\mathcal{C} = \{s_1, \ldots, s_M\}$ be an M-symbol constellation with minimum squared Euclidean separation $d_{\min}^2 = \min_{i \neq j} \|s_i - s_j\|^2$. A nearest-neighbour AWGN detector has pairwise error probability of the form

$$P(s_i \to s_j) = Q\left(\frac{\|s_i - s_j\|_2}{2\sigma} \right). \tag{56}$$

where σ^2 denotes per-real-dimension noise variance; the union bound is $P_e \leq (M-1)Q(d_{\min}/(2\sigma))$. A sphere-packing or coding upper bound limits *how large* a constellation/code can be at prescribed separation and dimension; it is not a constructive minimum-error design. AI-assisted stronger upper bounds [21] can guide feasibility screens for higher-dimensional codebooks, while actual new code designs require a separate search algorithm and decoder that can be implemented under bandwidth, peak-power and latency limitations. FunSearch cap-set constructions and improved kissing configurations [2,12] are possible construction seeds, but first the application must demonstrate why the corresponding arithmetic-progression or Euclidean-distance restriction reflects actual interference or modulation physics.

10. Preliminary Computational Pilot

This section reports preliminary model-level computational checks of the numerical-range and graph-restoration proposals. Calculations were executed using Python, SciPy, CVXPY and Clarabel as applicable; inputs and machine-readable results accompany the article. The synthetic models do not constitute experimental validation.

10.1. Robust Two-State Voltage-Regulation Surrogate

Consider the dimensionless small-signal surrogate $x_{k+1} = A_q x_k + B u_k + E d_k$ with

$$A_0 = \begin{bmatrix} 0.83 & 0.31 \\ -0.035 & 0.78 \end{bmatrix}, \quad B = \begin{bmatrix} 0.18 & 0 \\ 0.03 & 0.14 \end{bmatrix}, \quad E = \mathrm{diag}(0.04, 0.06). \tag{57}$$

The states represent normalised voltage error and a coupled power/frequency-related slow state; these matrices are a *synthetic computational surrogate*, not parameters identified from a specific grid-forming inverter. Three coupling cases are formed by multiplying both off-diagonal elements of A_0 by $s \in \{0.85, 1, 1.15\}$. The nominal LQR baseline uses $Q = \mathrm{diag}(4,1)$ and $R = 0.45 I_2$, with feedback $u_k = K x_k$. The proposed numerical-range (NR) method numerically seeks

$$\min_{K} \max_{q=1,2,3} w(A_q + BK), \qquad \|K\|_F \leq \|K_{\mathrm{LQR}}\|_F, \tag{58}$$

using the Ando LMI (10) with CVXPY 1.9.3 and CLARABEL 0.11.1. Feasibility and absolute/relative gap tolerances are 10^{-9}, maximum iterations 500; the deterministic convex problem requires no

© 2026 by the author(s). Distributed under a Creative Commons CC BY license.

Preprints.org | NOT PEER-REVIEWED | Posted: 23 November 2026 https://doi.org/10.20944/preprints202611.2339.v1

random restart. The gain norm constraint is a surrogate budget, not equal physical actuator effort. The solver returned optimal status in 10 iterations, $\gamma = 0.625265225$, with minimum block eigenvalue -2.98×10^{-10} (floating-point residual); the support-grid upper bound is recomputed from the returned gain. The gain is

$$K = \begin{bmatrix} -1.270751 & -1.067232 \\ -0.343905 & -1.024697 \end{bmatrix}.$$

The complete unrounded gain and all solver settings are in the supplementary JSON. As a unit check the same SDP was solved for F_0 and 15 seeded random complex matrices of dimensions 2, 3 and 4; the maximum absolute discrepancy from a 16384-angle support calculation was 3.43×10^{-8} and all SDP values lay within the discretisation envelopes up to solver tolerance. The support calculation and PSD residual are numerical checks, not an exact-arithmetic SDP certificate.

To verify the numerical radius independently of this optimisation, use M support angles and define $\widehat{w}_M(F) = \max_j \lambda_{\max}(H_{2\pi j/M}(F))$. The Lipschitz estimate gives

$$\widehat{w}_M(F) \le w(F) \le \widehat{w}_M(F) + \frac{\pi \|F\|_2}{M} =: \overline{w}_M(F). \tag{59}$$

All displayed upper bounds use $M = 4096$; hence $\overline{w}_M(F) < 1$ is a certified sufficient condition, conditional on the exact stated linear model. By Berger's 1965 power inequality it *already* yields the factor-two envelope $\|F^k\|_2 \le 2\overline{w}_M(F)^k$ for $k \ge 1$ [8]. The angle-grid computation in this pilot is retained only as independent post-hoc checking; the implemented design uses Ando's exact LMI (10). The upper envelope remains an a-posteriori check independent of SDP optimality.

The matched-budget direct spectral-norm baseline minimises γ subject to $\|K\|_F \le b$ and

$$\begin{bmatrix} \gamma I & F_q(K) \\ F_q(K)^T & \gamma I \end{bmatrix} \succeq 0, \quad \forall q.$$

Common-metric Lyapunov synthesis uses the formulation in Section 5.4 with $\|Z\|_F \le b$. The rate grid is $0.62, 0.63, \ldots, 0.92$; for each feasible rate the metric condition bound is minimised. The returned gains are screened by the recomputed bound at $k = 2$. The selected target rate is 0.64, the recomputed common contraction 0.638761 and $\sqrt{\kappa(P)}$ approximately one. This is a conservative gain-budget formulation, not an exact solution of the original norm-constrained joint synthesis problem.

Table 6. Two-statesurrogate, worst over three vertices. All controlled gains meet the same Frobenius upper budget. $\overline{w}_M$ is the certified support-grid upper bound. Peak after the first sample excludes $k = 1$.

Controller	$\|K\|_F$	$\max \rho$	$\max \overline{w}_M$	$\max \|F\|_2$	Peak $k = 2{:}40$
Open loop	0.00000	0.81348	0.96585	0.98917	0.96791
LQR	1.98042	0.61218	0.65677	0.67384	0.45160
Ando SDP	1.98042	0.61990	0.62576	0.63920	0.40788
Spectral norm SDP	1.98042	0.62118	0.63176	0.63733	0.40586
Common-P SDP	1.97429	0.62140	0.63085	0.63876	0.40746

All five peak values over $k = 1, \ldots, 40$ occur at $k = 1$, with no amplification above unity. The direct spectral-norm design achieves 0.63733, versus 0.63920 for Ando and 0.67384 for LQR. The spectral-norm design also has the smallest observed peak over $k = 2, \ldots, 40$. Thus the earlier improvement over LQR is not attributable specifically to numerical-radius synthesis. At the tested budget, this is a neutral result for Ando; the common-metric baseline is competitive. The comparison does not match real actuator constraints or optimal regulation costs.

For contrast, $F_* = \left[\begin{smallmatrix} 0.55 & 0.88 \\ 0 & 0.55 \end{smallmatrix}\right]$ has $\rho = 0.55$, $w = 0.99$, $\|F_*\|_2 = 1.14434$ and $\|F_*^2\|_2 = 1.05476$. The spectral-norm power estimate $\|F_*\|_2^k$ grows while the Berger envelope $2w(F_*)^k$ decays. This analytically transparent example illustrates a domain where the numerical-radius certificate is informative, not a claim of superior synthesis or a sharper bound than all Lyapunov alternatives.

© 2026 by the author(s). Distributed under a Creative Commons CC BY license.

Preprints.org | NOT PEER-REVIEWED | Posted: 23 November 2026 https://doi.org/10.20944/preprints202611.2339.v1

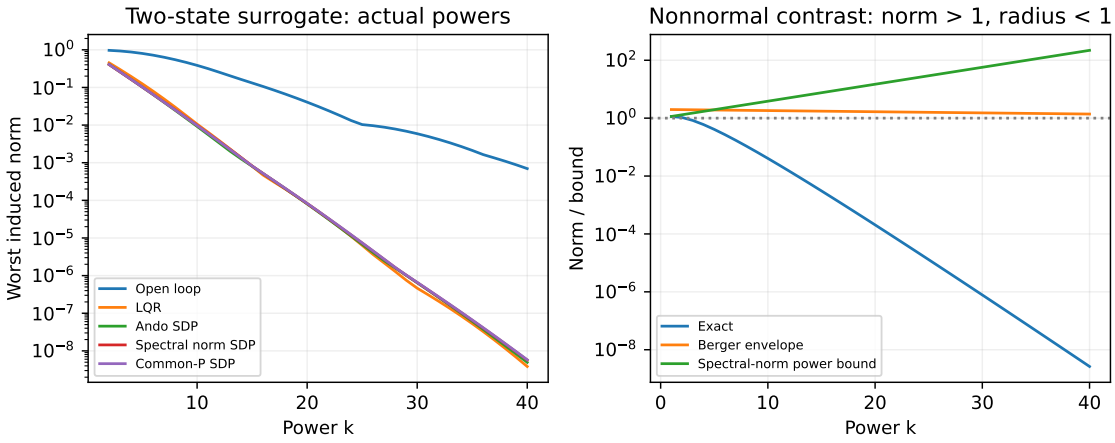


Figure 5. Left: induced powers for the matched-budget two-state surrogate, starting at $k = 2$. Right: contrasting stable nonnormal matrix with numerical radius below unity but induced gain above unity. The latter exhibits genuine finite-horizon amplification.

10.2. Six-State LCL Electrical Model: A Negative and Positive Certificate Test

To expose higher-order nonnormal dynamics, the synchronous-frame LCL model of (5) is discretised exactly under zero-order hold. The fixed-frequency physical parameters are $L_f = 1.8\,\mathrm{mH}$, $C_f = 20\,\mu\mathrm{F}$, $R_f = 0.10\,\Omega$, $R_g = 0.08\,\Omega$, $T_s = 50\,\mu\mathrm{s}$, $f = 50\,\mathrm{Hz}$, and grid-side inductance $L_g \in \{0.8, 1.2, 1.8\}$ mH. Converter and grid-voltage perturbations are scaled by 325 V. Write the physical states as $x_{mphys} = Dx$ with $D = 0.85\,\mathrm{diag}(L_f^{-1/2}, L_f^{-1/2}, C_f^{-1/2}, C_f^{-1/2}, L_{g0}^{-1/2}, L_{g0}^{-1/2})$, $L_{g0} = 1.2$ mH. Numerically $D = \mathrm{diag}(20.03469, 20.03469, 190.06578, 190.06578, 24.53739, 24.53739)$. For each fixed L_g use $T = \mathrm{diag}(1, 1, 1, 1, \sqrt{L_g/L_{g0}}, \sqrt{L_g/L_{g0}})$ and $F_e = TFT^{-1}$ when measuring amplification. These *scenario-specific norms* are not a common metric for arbitrary parameter switching.

Three cases are evaluated: zero feedback, nominal-model discrete LQR with $Q = \mathrm{diag}(1, 1, 5, 5, 1, 1)$ and $R = 0.08 I_2$, and physically interpretable passive virtual damping $\delta v_{id} = -R_v i_{fd}$, $\delta v_{iq} = -R_v i_{fq}$ with $R_v = 10\,\Omega$. Table 7 reports the worst case over the three fixed-grid scenarios.

Table 7. Six-state LCL model; three fixed inductance cases in scenario-specific energy coordinates; synthetic. $\widehat{w}_M$ is the sampled lower estimate, $\overline{w}_M$ is the certified upper envelope. B and L denote Berger and fixed-gain Lyapunov bounds at $k = 1, N$; peak excludes $k = 0$.

Controller	$\max \rho$	$\max \widehat{w}_M$	$\max \overline{w}_M$	B(1)	B(N)	L(1)	L(N)	Peak
Open loop	0.99875	0.99876	0.99952	1.99905	1.90698	1.00110	0.94097	0.99997
LQR	0.81625	1.15414	1.15540	2.31081	3.75e+06	3.07711	0.00018	1.67828
Virtual damping	0.95561	0.98474	0.98551	1.97102	0.46476	1.30031	0.12580	1.00134

The open loop already satisfies $\overline{w}_M < 1$ (0.99952), consistent with its dissipative energy dynamics; thus certifying virtual damping does not establish a new stability mechanism. At $k = 100$ the open-loop Berger bound is approximately 1.91, too weak to demonstrate useful settling. For LQR, $\overline{w}_M > 1$ makes this sufficient decay test inconclusive despite Schur stability; the Lyapunov bound at $k = 100$ is much more discriminating. Virtual damping lowers the worst numerical-radius bound to 0.98551 but has a larger actual short-horizon induced peak than the open loop. The fixed-gain Lyapunov results use the same scenario-specific energy coordinates, with $N = 100$; they do not imply a common switching metric. The LQR and passive voltage-step trajectories settle near 3.2 V, not zero reference error; a single trajectory's voltage overshoot is not the induced state norm. These results are negative or exploratory comparisons, not evidence of superior inverter control. Actuator saturation, droop/VSM dynamics, digital delay and switching nonlinearity remain outside the calculation.

© 2026 by the author(s). Distributed under a Creative Commons CC BY license.

Preprints.org | NOT PEER-REVIEWED | Posted: 23 November 2026 https://doi.org/10.20944/preprints202611.2339.v1

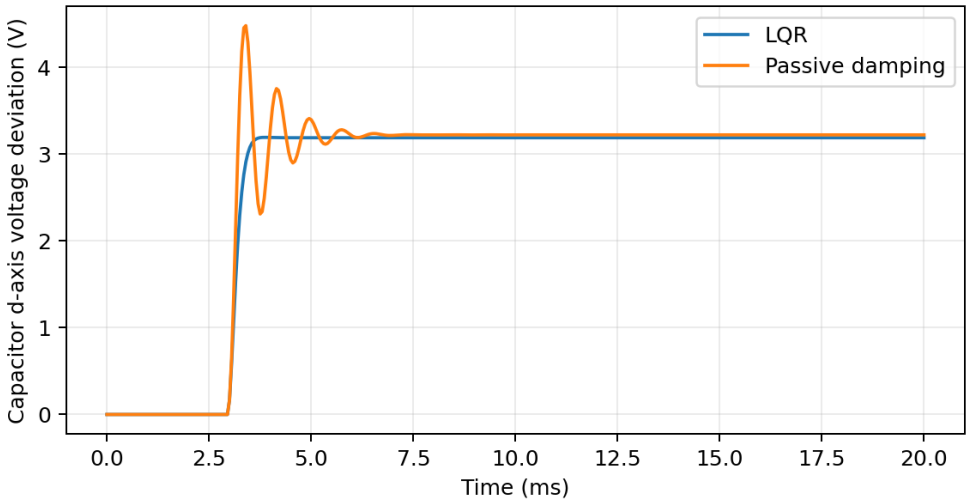


Figure 6. Synthetic fixed-frequency averaged LCL capacitor-voltage perturbation for one 1% grid-voltage change. Three fixed inductance cases are examined in the table; this nominal waveform is neither statistical evidence nor a complete grid-forming inverter.

10.3. Constructive Cycle Cover and Synthetic Radial Feeder Restoration

An eight-node communications test network comprises the ring $1 \to 2 \to \cdots \to 8 \to 1$ with the chord $(1,5)$. A cycle double cover is explicitly realised by the outer eight-cycle and the two five-edge cycles $1 \to 2 \to 3 \to 4 \to 5 \to 1$ and $1 \to 8 \to 7 \to 6 \to 5 \to 1$. Each of the nine edges appears *exactly twice*. This is a finite combinatorial verification of one simple instance of the recent graph result [6,7], not a claim that the general theorem is needed to construct this ring.

Under exhaustive individual communication-edge deletion, a seven-link chain connects on average 42.86% of the seven non-root nodes, whereas an eight-link ring and nine-link ring-plus-chord each preserve all seven nodes after any single-edge failure. This advantage comes from *extra redundant links* and cannot isolate a special benefit of cycle covers compared with ordinary two-edge-connectivity methods. Fig. 7 illustrates the explicit constructive cover.

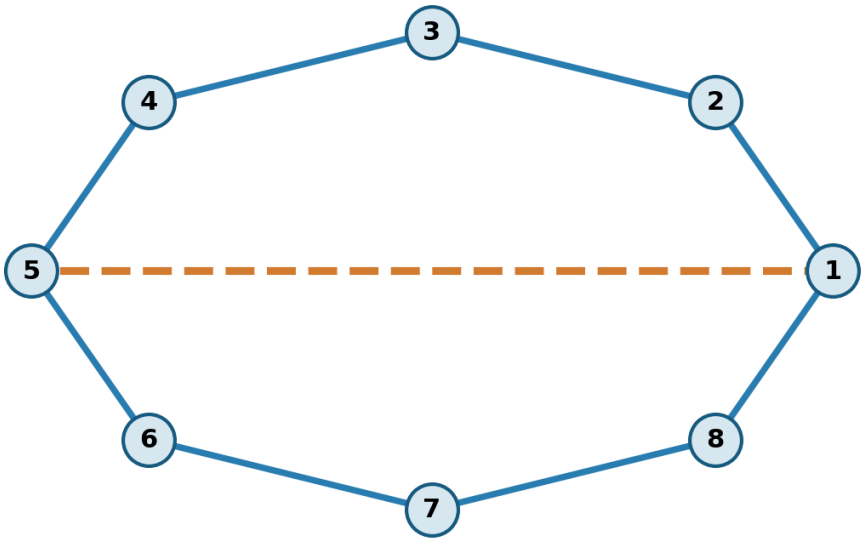


Figure 7. Finite, explicitly checked synthetic communication graph cycle cover: outer ring and two chord-bounded cycles. The distinct radial power graph is not coupled to packet failures; no statistical or field validation.

© 2026 by the author(s). Distributed under a Creative Commons CC BY license.

Preprints.org | NOT PEER-REVIEWED | Posted: 23 November 2026 https://doi.org/10.20944/preprints202611.2339.v1

A separate *synthetic* eight-bus radial power feeder is then evaluated, with seven normally closed consecutive branches, three candidate ties $(1,5)$, $(2,6)$ and $(3,8)$, and assigned per-unit line impedances/loads supplied in the source code. In response to three distinct line faults, all possible seven-edge candidate spanning trees are enumerated. Connectivity, first-order balanced LinDistFlow voltage range 0.95–1.05 p.u., a simplified branch apparent-power threshold and a switching-cost surrogate are enforced. The search only considers *all-bus restoration* and does not represent load-shedding optimisation, nonlinear AC power flow or timing-limited SCADA control. Table 8 records the checked outcomes.

Table 8. Synthetic eight-bus power restoration, three enumerated faults only (not a random sample). No-switch lost load versus voltage-feasible all-bus radial switching; no confidence interval or CDC-specific benefit is inferred.

Fault	Lost load, before	Lost load, after	Min V	Switch ops
2–3	0.295 p.u.	0	0.99029	1
4–5	0.195 p.u.	0	0.99233	1
6–7	0.095 p.u.	0	0.98837	1

The three feasible restorations demonstrate a working small network-enumeration and screening mechanism. They do *not* establish a CDC-specific improvement: feeder reconfiguration alone can deliver the same outcomes, and the communication graph is evaluated separately. A future claim about communication-assisted restoration requires a linked cyber–physical switching model, explicit packet-delay and command-failure scenarios, cost-matched baselines, and the published IEEE 33/69-bus feeder parameters [41].

10.4. Reproduction, Validity Boundaries and Next Validation Tier

The supplementary archive contains the executed reference scripts, seeds, solver settings, numerical CSV files and model definitions. For deterministic LCL and feeder cases, the values apply only to the specified scenarios. Physical modelling, actuator saturation, delay and coupled feeder-communications tests remain necessary before technology-level performance claims.

11. A Unified Engineering Research Programme

11.1. Novelty and Risk Ranking

This review recommends beginning with directions that have a *direct mathematical guarantee* and an accessible engineering model. Table 9 distinguishes new mathematical tools from conjectured performance gains. In the ranking, theory readiness refers to availability of a precise result, not engineering technology readiness level.

© 2026 by the author(s). Distributed under a Creative Commons CC BY license.

Preprints.org | NOT PEER-REVIEWED | Posted: 23 November 2026 https://doi.org/10.20944/preprints202611.2339.v1

Table 9. Prioritised proposed engineering research programmes; advantages remain hypotheses until benchmarked.

Proposed programme	Mathematical relationship	Distinguishing possible contribution	Hardest validation risk
Converter polynomial-response certification	Classical Berger power inequality; published Crouzeix–Palencia polynomial bound	Exact Ando LMI and proposed polynomial/transfer-function evaluation	Must outperform Lyapunov, H_∞ and physical test baselines
Communication-aware feeder recovery	Structural graph theorem plus new model	CDC-informed redundancy with actual DistFlow and packet-delay constraints	Does CDC improve beyond simpler 2-edge-connectivity/path designs?
Adaptive MIMO detection	Hardness result; exact ML cost certificates	Tail-latency constrained algorithm selection with verified gaps to ML	Generalisation over channels; FPGA silicon cost
Identifiable nonlinear digital twins	Classical strong monotonicity and global inverse results	Proposed robust measurement-projection selection with domain-wide Jacobian enclosures	Condition may fail or be conservative for real AC/battery physics
Hadamard multiplexed sensing	Direct orthogonality identity	Calibrated finite-size coding design using newly available orders	Practical bipolar, analogue and timing limits
Last-iterate robust optimisation	Formal theorem under convex–concave assumptions	Certified convergence for physically meaningful convex surrogates	Relaxation gap and discrete switching

11.2. Common Evaluation Design and Reproducibility

For a credible engineering paper, the data and implementations must be sufficiently detailed to reproduce claimed performance. Every study should state system topology, ratings, sample time, noise/uncertainty models, finite numerical precision, solver version, baseline tuning budget and random seeds. A comparison should use paired operating scenarios to reduce variance; when stochastic channels or fault samples are involved, supply empirical means, medians, tail percentiles, uncertainty intervals and the number of independent runs. For optimisation, report solver termination gap and feasibility residuals rather than only an objective value. To guard against false novelty, compare against the *strongest relevant existing method*: robust LMI/linear-quadratic control for the numerical-range project; minimum cut, k-edge-connectivity, link-disjoint paths and classic distribution reconfiguration for the CDC project; MMSE, fixed K-best and sphere decoding for the MIMO project; and multiple-start state estimation/interval observers for the inverse-model project. Always distinguish improvements in the bound from improvements measured in the actual closed-loop system.

11.3. Traceable Experiment Checklist

A proposed project can be implemented in the following sequence. **Step 1:** record the verified mathematical statement, the exact form of its source, and assumptions. **Step 2:** derive the mathematical mapping for the physical system using dimensionally consistent variables. **Step 3:** establish a theorem-to-design implication (or explicitly state that one is unavailable). **Step 4:** implement the new mathematical constraint or heuristic in a reproducible numerical model. **Step 5:** demonstrate feasibility on at least one transparent analytical or small benchmark instance. **Step 6:** compare against strong published alternatives with identical operating scenarios. **Step 7:** run uncertainty, model-mismatch, solver-accuracy and finite-precision sensitivity analyses. **Step 8:** if the idea survives, validate with a real-time platform or laboratory equipment. The two-state and LCL reference tests provide only limited model-level evidence; neither establishes an improvement over state-of-the-art methods across representative physical operating conditions.

12. Limitations, Responsible Attribution, and Research Integrity

The available mathematical evidence is heterogeneous. Expert-checked expositions, Lean-checked statements, exact finite objects and organisational announcements are not equivalent. Some formal proof targets resolve variants that are strictly weaker than their celebrated parent conjectures. At-

© 2026 by the author(s). Distributed under a Creative Commons CC BY license.

Preprints.org | NOT PEER-REVIEWED | Posted: 23 November 2026 https://doi.org/10.20944/preprints202611.2339.v1

tributing a proof entirely to AI can also omit essential human choices: recognising the open problem, supplying a representation, constructing a decisive prompt, repairing mathematical assumptions, recognising rediscovery, and writing a rigorous exposition. Conversely, it would be incorrect to call AI-assisted construction merely a search heuristic when the published work contains a new human-checked theorem or exact certificate. The article therefore records both novelty type and AI role rather than reporting a single sensational solved-problem count [1,10].

The engineering formulations in Sections 5–8 are proposed translations using established mathematical tools. They are mathematically explicit and have derivations within stated models, and are accompanied by small Python-reference numerical pilots, but neither the controller nor the cyber–physical restoration scheme has undergone broad parametric validation, physical verification, or hardware-in-the-loop testing. The matrix-power inequality is classical (Berger), while the general polynomial spectral-set theorem provides a different bound; the graph cycle cover is not equivalent to two fully independent communication paths; CVP hardness does not itself provide a detector speed-up; and the Jacobian counterexample does not disprove global invertibility for every practical real sensor map. Likewise, a new Hadamard order does not guarantee superior SNR in all front ends. Publication-quality results require both mathematical checking and engineering experiments.

13. Conclusion

AI-assisted mathematics has matured from generating candidate examples to providing proofs, counterexamples, formal certificates and constructions for problems that remained open for years or decades. This paper catalogued 51 selected findings: 51 heterogeneous findings across 49 target families, classified by result type and evidence level. These counts reflect a curated dataset, not the number of conjectures accepted as settled by the mathematical community. The full catalogue supplies mathematical background, AI participation, primary evidence and candidate links to many branches of engineering, rather than treating the existence of an AI proof as an automatic engineering innovation. The most testable, not yet established research directions are (i) classical numerical-radius synthesis and general polynomial-response evaluation for sampled inverter networks, (ii) survivable communication topology with power-flow-feasible restoration, (iii) complexity-aware MIMO receivers with instance-specific optimality certificates, and (iv) globally identifiable nonlinear sensing and digital twins using strong monotonicity. The article derives sufficient mathematical conditions for each applicable direction and illustrates selected calculations without fabricating experimental results. An eventual original technology contribution would require a rigorously reproduced comparison of the proposed methods against established control, optimisation, communications and state-estimation baselines, with hardware validation where practical.

Supplementary Materials: The following supporting information can be downloaded at the website of this paper posted on Preprints.org.

Funding: This research received no external funding.

Institutional Review Board Statement: Not applicable.

Informed Consent Statement: Not applicable.

Data Availability Statement: The synthetic data, scripts, model settings, solver diagnostics and 51-entry source audit are provided as supplementary reproducibility files. They contain no participant or proprietary data; no laboratory dataset was used. The code, CSV and JSON files, together with reproduction instructions, are included in the accompanying supplementary materials.

Acknowledgments: The idea, design, and structural framework of this manuscript were developed entirely by the author. The author acknowledges the use of ChatGPT (OpenAI, November 2026) for assistance with writing preparation, code generation, and numerical simulations. The author retains sole authorship and full responsibility for the content. [53].

© 2026 by the author(s). Distributed under a Creative Commons CC BY license.

Preprints.org | NOT PEER-REVIEWED | Posted: 23 November 2026 https://doi.org/10.20944/preprints202611.2339.v1

Appendix A. Mathematical Notation and Common Pitfalls

Table A1. Distinct symbol roles; context must be stated in every section.

Symbol	Meaning and possible collision
$w(F), \rho(F), \gamma$	Numerical radius; spectral radius; certificate bound γ (also CVP factor or optimisation weight in context).
F, K, P	Discrete transition, feedback gain, and Lyapunov metric.
$H_q, H_\theta, H_{\text{MIMO}}$	Ando auxiliary Hermitian matrix, support-function matrix, radio channel.
L_f, L_g, L	Physical inductances and measurement projection (not the same).
B, E	Input/disturbance matrices, with energy denoted E_{tr} if needed.
$Q_{\text{nom}}, Q_i, Q(\cdot)$	Battery charge capacity (A s), reactive power, and Gaussian-tail function.
$x, x^p, x^{(r)}$	Dynamic state, energized-edge status, and path-use binaries.
$S, \mathcal{S}$	State scaling, graph cut set or symbol constellation (as defined locally).

Throughout, $\|\cdot\|_2$ denotes the spectral or Euclidean norm as appropriate, $\preceq$ and $\succeq$ denote Hermitian semidefinite order, and $\mathcal{W}(F)$ denotes the complex numerical range of F. Note three subtle distinctions: (a) $\rho(F) < 1$, where ρ is the spectral radius, is necessary and sufficient for Schur stability; $w(F) < 1$ is a stronger, sufficient condition used for the transparent bound in (2). (b) A bridgeless installed communication graph satisfies the hypotheses of the reported CDC claim, but a distribution feeder's energised topology may be radial. (c) A full-rank pointwise Jacobian gives local regularity; it is not a global one-to-one theorem. These distinctions are central to engineering use of the mathematical advances.

Appendix B. Practical Software Implementation Skeletons

Appendix B.1. Numerical-Radius and Polynomial-Response Controller

Implement Ando's exact Hermitian block LMI (10) with one auxiliary H_q per genuine uncertainty vertex; no support-angle grid is required for synthesis. Verify each resulting $w(F_q)$ by an independent support-function scan. Separately evaluate the actual polynomial $p(F)$ or the transfer resolvent, including the published Crouzeix–Palencia polynomial envelope, shifted termwise and Lyapunov comparisons, and the elementary resolvent bound. Use common physical units and explicit actuator limits. An unsuccessful sufficient certificate does not prove the plant uncontrollable.

Appendix B.2. Grid Survivability Optimisation

Build a layer for candidate communication links, a layer for electrical feeders and a mapping from buses and controllers to communication devices. First solve 2-edge-connectivity augmentation using (17); then attempt a cycle double cover as a diagnostic; then compute disjoint controller paths subject to delay, followed by feasible power restoration. In Monte Carlo experiments, correlate failures through explicit shared-risk groups to avoid inflated reliability estimates. An ablation study must remove just the CDC feature while retaining the same two-edge-connectivity and number of physical links; otherwise it cannot isolate the theorem-related contribution.

Appendix B.3. Wireless Detector

Generate whitened candidate metrics using (30) and (31). Use exact exhaustive enumeration for tiny dimensions to provide ground truth and a branch-and-bound oracle for moderate dimensions. Every time-limited run returns detected symbols, a binary exactness flag, a rigorous candidate cost upper bound and (if available) a valid lower bound. This separation allows empirical BER and latency improvements without falsely labelling an approximate solution mathematically optimal.

Appendix B.4. Nonlinear Twin Identifiability

Determine a physically feasible, convex state region D. Construct derivative enclosures $J_h(D)$ analytically or by interval arithmetic. Search for a projection L satisfying (37) across the *entire* region,

© 2026 by the author(s). Distributed under a Creative Commons CC BY license.

Preprints.org | NOT PEER-REVIEWED | Posted: 23 November 2026 https://doi.org/10.20944/preprints202611.2339.v1

not just training samples. If infeasible, use domain partitioning with separate certificate regions and explicit disambiguation logic; do not silently combine multiple local certificates into a globally unique inverse. Report both the proven identifiable domain and un-certified operating points.

Appendix C. Status and Citation Audit for the Catalogue

A citation to an organisation's release identifies an attributed reported result. E1 entries are the refereed FunSearch study and five independent written expositions or exact-construction checks (unit distance, CDC, Erdős–Sós, Hadamard, matrix multiplication). The latter are preprints, not equivalent to journal acceptance. E2 requires corroborated, version-specific proof compilation or exact checking; no such grade is assigned in this audit. E3 includes all ten organisational themes (11 rows), all four Adamczewski–Bloom rows, unrebuilt formal reports, and the Crouzeix and Sendov reports. Townsend and Greenbaum's SIAM News commentary and Tao's blog are valuable expert assessments, but neither is a peer-reviewed proof verification. No Lean build, theorem identifier/assumption audit or gap-free formal proof compilation was performed; linked conjecture statement files may contain `sorry`. The companion 51-row CSV records the source type, available identifier/version, evidence rationale and engineering direction. All claims are a snapshot at 14 November 2026; targeted bibliography checks were updated 15 November 2026. The mathematical and numerical evidence labels must not be conflated.

References

1. Tsoukalas, G.; Kovsharov, A.; Shirobokov, S.; et al. Advancing Mathematics Research with AI-Driven Formal Proof Search, 2026, [2605.22763].
2. Romera-Paredes, B.; et al. Mathematical discoveries from program search with large language models. *Nature* **2024**, *625*, 468–475. https://doi.org/10.1038/s41586-023-06924-6.
3. Jin, S. The Numerical Range Is a 2-Spectral Set, 2026. Manuscript and author-maintained proof source.
4. Townsend, A.; Greenbaum, A. The Neurosurgery Resident Who Proved Crouzeix's Conjecture. *SIAM News* **2026**, *59*.
5. Crouzeix, M.; Palencia, C. The Numerical Range is a $(1+\sqrt{2})$-Spectral Set. *SIAM Journal on Matrix Analysis and Applications* **2017**, *38*, 649–655. https://doi.org/10.1137/17M1116672.
6. Oum, S. A proof of the cycle double cover conjecture by OpenAI: An exposition, 2026, [2607.16356].
7. Geelen, J. OpenAI's proof of the Cycle Double Cover Theorem, 2026, [2607.15399].
8. Berger, C.A. A Strange Dilation Theorem. *Notices of the American Mathematical Society* **1965**, *12*, 590. Research announcement and classical power inequality.
9. Novikov, A.; et al. AlphaEvolve: A coding agent for scientific and algorithmic discovery, 2025, [2506.13131].
10. Feng, T.; Trinh, T.; Bingham, G.; et al. Semi-Autonomous Mathematics Discovery with Gemini: A Case Study on the Erdős Problems, 2026, [2601.22401].
11. Sawhney, M.; Sellke, M. Early experiments in accelerating science with GPT-5: Erdős problem 848. OpenAI research report, 2025. Contains the named authors' account of the asymptotic result, not a separate journal article.
12. Georgiev, B.; Gómez-Serrano, J.; Tao, T.; Wagner, A.Z. Mathematical exploration and discovery at scale, 2025, [2511.02864]. Preprint, version 3.
13. Sothanaphan, N. Resolution of Erdős Problem #728: a writeup of Aristotle's Lean proof, 2026, [2601.07421].
14. The Erdos Problems Project. Problem 729: AI-assisted proof and formalisation notes, 2026. Open problem registry, checked 14 November 2026.
15. Chen, E.; Cummins, C.; Grubisic, D.; et al. Fel's Conjecture on Syzygies of Numerical Semigroups, 2026, [2602.03716]. Lean/Mathlib proof reported; 2026 preprint revised after referee reports.
16. Alon, N.; Bloom, T.F.; Gowers, W.T.; Litt, D.; Sawin, W.; Shankar, A.; Tsimerman, J.; Wang, V.; Wood, M.M. Remarks on the disproof of the unit distance conjecture, 2026, [2605.20695]. Human-verified exposition of an AI-generated counterexample.
17. Konz, N. Claude Tackles Borsuk: Independent Rediscovery and Exact Certificate, 2026. Project page credits Max Grinsztajn for priority; not peer-reviewed.
18. Ji, Y. An AI Generated Counterexample to Borsuk Problem in Dimension 63, 2026, [2608.12561].

© 2026 by the author(s). Distributed under a Creative Commons CC BY license.

Preprints.org | NOT PEER-REVIEWED | Posted: 23 November 2026 https://doi.org/10.20944/preprints202611.2339.v1

19. Gao, S. Counterexamples to the Jacobian conjecture in dimensions greater than two, 2026, [2608.00222]. Revised 4 November 2026, v2.
20. Tao, T. A digestion of the proof of Sendov's conjecture, 2026. Expert blog exposition, not peer-reviewed.
21. OpenAI. Ten advances in mathematics and theoretical computer science, 2026. Collection of individual AI-generated proofs and improved bounds; formal verification reported by authors.
22. Adamczewski, T.; Böhmler, B.; Marczinzik, R. A counterexample to Köthe's conjecture and a question of Rowen, 2026, [2609.07996].
23. Riordan, O.; Scott, A. A short proof of the Erdős–Sós conjecture, 2026, [2609.15893]. Preprint, version 3; revised 8 October 2026.
24. Adamczewski, T.; Bloom, T.F. FrontierMath Erdős, 2026, [2609.25050].
25. Surina, A.; Suggala, A.; Tsoukalas, G.; Kovsharov, A.; Shirobokov, S.; Ruiz, F.J.R.; Kohli, P.; Chaudhuri, S. An Improved Last-Iterate Convergence Rate for Anchored Gradient Descent Ascent, 2026, [2604.03782].
26. Zhang, X.; Zhou, Q. Chernoff's Density Is Strongly Log-Concave, 2026, [2607.18619].
27. Egan, R.; Kotsireas, I.; London, S.; Catháin, P.Ó. Recent progress in the construction of Hadamard matrices, 2026, [2610.27175].
28. OpenAI. An Upper Bound of 9/4 for the Matrix Multiplication Exponent, 2026. Preprint, 2 October 2026.
29. Pass, R. Matrix Multiplication from Polynomial Packings: A Constructive and Elementary Proof of $\omega \leq 9/4$, 2026, [2610.28627]. Version 2, 30 October 2026.
30. Lü, H. Polynomial Separation of a Shared Tensor Leg and Matrix Multiplication in Arbitrary Characteristic, 2026, [2610.18914]. Preprint, 12 October 2026.
31. Amanov, A.; van den Berg, M.; Zuiddam, J. Multiplying matrices via polynomials: exposition and barriers, 2026, [2610.30054]. Preprint, 21 October 2026.
32. Alman, J.; Williams, V.V. Truly Subquadratic 3SUM and Truly Subcubic APSP via Triangles in Sparse Lopsided Graphs, 2026, [2610.06783].
33. Dujella, A. Elliptic curves with high rank: records and corrections, 2026. Independent record registry; AI-assisted construction reports to be checked against explicit certificates.
34. Trefethen, L.N.; Embree, M. *Spectra and Pseudospectra: The Behavior of Nonnormal Matrices and Operators*; Princeton University Press: Princeton, NJ, USA, 2005.
35. Ando, T. Structure of Operators with Numerical Radius One. *Acta Scientiarum Mathematicarum* **1973**, *34*, 11–15. https://doi.org/10.1007/BF03549843.
36. Bhatia, R.; Jain, T. The Numerical Radius and Positivity of Block Matrices. *Linear Algebra and its Applications* **2023**, *656*, 463–482. https://doi.org/10.1016/j.laa.2022.10.009.
37. Grover, W.D.; Stamatelakis, D. Cycle-oriented distributed preconfiguration: Ring-like speed with mesh-like capacity for self-planning network restoration. In Proceedings of the Proceedings of IEEE ICC, 1998, pp. 537–543.
38. Stamatelakis, D.; Grover, W.D. IP Layer Restoration and Network Planning Based on Virtual Protection Cycles. *IEEE Journal on Selected Areas in Communications* **2000**, *18*, 1938–1949. https://doi.org/10.1109/49.887914.
39. Stamatelakis, D.; Grover, W.D. Theoretical Underpinnings for the Efficiency of Restorable Networks Using Preconfigured Cycles (p-cycles). *IEEE Transactions on Communications* **2000**, *48*, 1262–1265. https://doi.org/10.1109/26.864163.
40. Jain, K. A Factor 2 Approximation Algorithm for the Generalized Steiner Network Problem. *Combinatorica* **2001**, *21*, 39–60. https://doi.org/10.1007/S004930170004.
41. Baran, M.E.; Wu, F.F. Network reconfiguration in distribution systems for loss reduction and load balancing. *IEEE Transactions on Power Delivery* **1989**, *4*, 1401–1407. https://doi.org/10.1109/61.25627.
42. Farivar, M.; Low, S.H. Branch Flow Model: Relaxations and Convexification—Part I. *IEEE Transactions on Power Systems* **2013**, *28*, 2554–2564. https://doi.org/10.1109/TPWRS.2013.2255317.
43. Menger, K. Zur allgemeinen Kurventheorie. *Fundamenta Mathematicae* **1927**, *10*, 96–115.
44. Aharonov, D.; Regev, O. Lattice Problems in NP ∩ coNP. *Journal of the ACM* **2005**, *52*, 749–765. https://doi.org/10.1145/1089023.1089025.
45. Jaldén, J.; Ottersten, B. On the Complexity of Sphere Decoding in Digital Communications. *IEEE Transactions on Signal Processing* **2005**, *53*, 1474–1484. https://doi.org/10.1109/TSP.2005.843746.
46. Hassibi, B.; Vikalo, H. On the sphere-decoding algorithm I. Expected complexity. *IEEE Transactions on Signal Processing* **2005**, *53*, 2806–2818. https://doi.org/10.1109/TSP.2005.850352.

© 2026 by the author(s). Distributed under a Creative Commons CC BY license.

Preprints.org | NOT PEER-REVIEWED | Posted: 23 November 2026 https://doi.org/10.20944/preprints202611.2339.v1

47. Barbero, L.G.; Thompson, J.S. Fixing the complexity of the sphere decoder for MIMO detection. *IEEE Transactions on Wireless Communications* **2008**, *7*, 2131–2142. https://doi.org/10.1109/TWC.2008.060378.
48. Pinchuk, S. A counterexample to the strong real Jacobian conjecture. *Mathematische Zeitschrift* **1994**, *217*, 1–4. https://doi.org/10.1007/BF02571929.
49. Gale, D.; Nikaido, H. The Jacobian Matrix and Global Univalence of Mappings. *Mathematische Annalen* **1965**, *159*, 81–93. https://doi.org/10.1007/BF01360282.
50. Ortega, J.M.; Rheinboldt, W.C. *Iterative Solution of Nonlinear Equations in Several Variables*; Academic Press: New York, 1970. https://doi.org/10.1016/C2013-0-11263-9.
51. Abur, A.; Expósito, A.G. *Power System State Estimation: Theory and Implementation*; CRC Press: Boca Raton, FL, USA, 2004. https://doi.org/https://doi.org/10.1201/9780203913673.
52. Yoon, T.; Ryu, E.K. Accelerated Algorithms for Smooth Convex–Concave Minimax Problems with $O(1/k^2)$ Rate on Squared Gradient Norm. In Proceedings of the Proceedings of the International Conference on Machine Learning, 2021, Vol. 139, pp. 12098–12109.
53. Springer Nature. AI Guidance for Researchers, Editors and Reviewers, 2026. Publisher policy consulted 14 November 2026; follow target journal requirements.

Disclaimer/Publisher's Note: The statements, opinions and data contained in all publications are solely those of the individual author(s) and contributor(s) and not of MDPI and/or the editor(s). MDPI and/or the editor(s) disclaim responsibility for any injury to people or property resulting from any ideas, methods, instructions or products referred to in the content.

© 2026 by the author(s). Distributed under a Creative Commons CC BY license.